Cavity Ringdown Laser Absorption Spectroscopy: History, Development, and Application to Pulsed Molecular Beams

J. J. Scherer,† J. B. Paul, A. O'Keefe,‡ and R. J. Saykally*

Department of Chemistry, University of California, Berkeley, California 94720, and Los Gatos Research, 1685 Plymouth Way, Mountain View, California 94043

Received December 2, 1993 (Revised Manuscript Received September 13, 1996)

Contents

I. Introduction

The measurement of electronic spectra of supersonically cooled molecules and clusters is a widely used approach for addressing many problems in chemistry. The most established techniques for making such measurements are laser-induced fluorescence (LIF) and resonance-enhanced multiphoton ionization (REMPI), and both have been employed very successfully in a large number of studies. However, both methods often fail for systems containing more than a few atoms, due to rapid internal conversion, predissociation, or other dynamical processes. Even for small systems, the vibronic band intensities are often contaminated by intramolecular relaxation dynamics; in such cases, these techniques cannot be used for reliable intensity measurements. For clusters that exhibit rapid photofragmentation, depletion spectroscopy can be employed quite effectively to measure their vibronic structure, but again, dynamic effects complicate the interpretation of spectra. The same considerations apply to other types of "action" spectroscopy.

It would often be preferable to measure the electronic spectra of molecules and clusters in direct absorption, as this approach is the most straightforward and accurate means of determining absolute vibronic band intensities and for accessing states that are invisible to LIF or REMPI. The problem, of course, is that direct absorption methods are generally orders of magnitude less sensitive than the "action" techniques and are, therefore, difficult to apply to transient species, such as clusters or radicals.

In this review, we describe a relatively new direct absorption technique that we have developed for measuring the electronic spectra of jet-cooled molecules and clusters with both high sensitivity and high spectral resolution. The method is based on measurement of the time rate of decay of a pulse of light trapped in a high reflectance optical cavity; we call it cavity ringdown laser absorption spectroscopy (CRLAS). In practice, pulsed laser light is injected into an optical cavity that is formed by a pair of highly reflective ($R > 99.9\%$) mirrors. The small amount of light that is now trapped inside the cavity reflects back and forth between the two mirrors, with a small fraction ($\sim 1 - R$) transmitting through each mirror with each pass. The resultant transmission of the circulating light is monitored at the output mirror as a function of time and allows the decay time of the cavity to be determined. A simple picture of the cavity decay event for the case where the laser pulse is temporally shorter than the cavity round trip transit time is presented in Figure 1. In this case, the intensity envelope of these discrete transmitted pulses exhibits a simple exponential decay. The time required for the cavity to decay to 1/e of the initial output pulse is called the "cavity ringdown" time. Determination of the ringdown time allows the absolute single pass transmission coefficient of the cavity to be determined with high accuracy, given the mirror spacing. The apparatus is converted to a sensitive absorption spectrometer simply by placing an absorbing medium between the two mirrors and recording the frequency dependent ringdown time of the cavity. Ideally, the ringdown time is a function of only the mirror reflectivities, cavity dimensions, and sample absorption. Absolute absorption intensities are obtained by subtracting the base-line transmission of the cavity, which is determined when the laser wavelength is off-resonance with all molecular transitions.

† IBM Predoctoral Fellow. Current address: Sandia National Laboratories, M/S 9055, Livermore, CA 94551-0969.
‡ Los Gatos Research.

S0009-2665(93)00048-2 CCC: $28.00

James J. Scherer was born and raised in Berkeley, CA. He received his Bachelors degrees in art and physics at the University of California at Berkeley, followed by a Doctoral degree in chemistry also at Berkeley. His research interests include spectroscopic studies of metal cluster species and free radicals.

Joshua B. Paul received his Bachelor's degree in Physics in 1991 from the University of California at Berkeley. As an undergraduate, he worked in Professor Saykally's laboratories helping to build the current cavity ringdown apparatus. When given the opportunity to join the Chemistry Graduate program at Berkeley, he gladly accepted, electing to continue his work on the ringdown project. Recently, he has switched from UV–visible studies to the mid-infrared, where he has employed ringdown toward the study of the O–H stretch fundamentals of water clusters and the N–H stretches of nucleotide base clusters. At 28 years of age, Josh will soon face the realities of life after Graduate School.

Because the cavity decay time is independent of the initial intensity that exits the cavity, CRLAS sensitivity is not seriously degraded by the large shot to shot intensity fluctuations common to pulsed lasers. With state-of-the-art data collection methods, a fractional absorption $(1 - I/I_o)$ of 3×10^{-7} per pass can be measured with a single laser pulse; signal averaging can be employed to improve this figure. While currently implemented from the ultraviolet to the mid-infrared regions, CRLAS is primarily limited to spectral regions by both the availability of highly reflective mirrors and suitable pulsed laser sources.

In this paper, we present an account of the theory, development, and applications of the CRLAS method, with emphasis on the specific application of pulsed molecular beam spectroscopy. In addition to a general review of CRLAS, experimental data are presented that demonstrate the simplicity, sensitivity, and generality of this powerful new spectroscopic tool.

Anthony O'Keefe is President of Los Gatos Research, a small R&D company located in the San Francisco area that is involved in government-funded laser research for aerospace applications. Prior to this position he was a partner and co-owner of Deacon Research, where he developed the Cavity Ringdown Absorption technique that forms the basis of the present work. He has worked to develop this technique from a laboratory curiosity to a widely recognized method of making ultra-high sensitivity spectroscopic measurements. Dr. O'Keefe received his B.S. degree in Chemistry from Beloit College in 1977 and his M.S. and Ph.D. degrees in physical chemistry from the University of California, Berkeley, in 1979 and 1981, respectively.

Richard Saykally was born in 1947 in Rhinelander, WI. He graduated from the University of Wisconsin—Eau Claire in 1970 and received his Ph.D. from UW—Madison in 1977 under the direction of R. C. Woods. After spending two years at NIST in Boulder as a NRC postdoctoral fellow with K. M. Evenson, he was appointed Assistant Professor at UC Berkeley in 1979. He has served as Vice-Chair of Chemistry from 1988 to 1991 and has been the thesis advisor for 30 Ph.Ds. He has received numerous honors and awards, including the Harrison–Howe Award, the Lippincott Prize for Vibrational Spectroscopy, the Bomem Michelson Award in Spectroscopy, the E. K. Plyler Prize for Molecular Spectroscopy, the Bourke Lectureship of the Royal Society of Chemistry, and a Humboldt Senior Scientist Award. He has been a Presidential Young Investigator and a Dreyfus Scholar and is a Fellow of the American Physical Society, the Optical Society of America, the Royal Society of Chemistry, and the American Academy of Arts and Sciences. He serves on the editorial boards of *The Journal of Chemical Physics*, *Molecular Physics*, *Chemical Physics Letters*, *The Review of Scientific Instruments*, *The Journal of Molecular Spectroscopy*, and *Spectroscopy*. Also recognized as an outstanding teacher, Professor Saykally has received the Berkeley Distinguished Teaching Award and was the co-director of Science for Science Teachers, a national program for secondary school teacher enhancement. He has published nearly 200 papers on subjects ranging from intermolecular forces and molecular ions to astrophysics and laser spectroscopy.

II. CRLAS History and Development

The history and development of the CRLAS technique dates back to the invention of the cw-based cavity attenuated phase shift (CAPS) method by J. M. Herbelin et al. in the early 1980's.[1] Although the

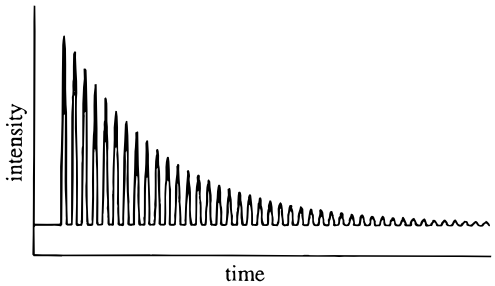

Figure 1. In the short pulse limit, discrete pulses of laser light leak out of the cavity with each pass. The intensity envelope of the resultant decay is approximated by a smooth exponential expression. Determination of the decay time allows the cavity losses or molecular absorption to be determined. Typical cavity decays consist of ten thousand such pulses.

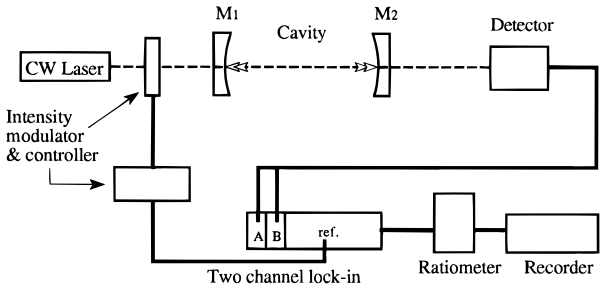

Figure 2. Cavity attenuated phase shift method (CAPS) experimental diagram. Modulated continuous wave laser light is coupled into a high-finesse optical cavity. Measurement of the resultant phase shift at the exit mirror allows the mirror reflectivities to be determined. In Herbelin's original work, a ring resonator was also used.

CAPS method, which was initially developed solely for the characterization of mirror reflectivities, is significantly different from the current pulsed cavity ringdown approach, it is to our knowledge the original experiment in which the cavity decay time (inferred from a measured phase shift) is used extract the single pass transmissivity (or reflectance) of an optical resonator. All subsequent developments that have led to the current cavity ringdown technique are based on modifications of this approach. It is worth reviewing the CAPS technique in some detail to illustrate both some limitations of CRLAS as well as potential future applications. Additionally, comparison of the two methods naturally leads to a discussion of the role of interference effects and cavity resonances that may be important in certain experimental regimes.

In the CAPS technique, the lifetime of a photon in a high-finesse optical resonator is inferred from the measured phase shift between the modulated input and output light of an optical cavity. In the original work, two and three mirror cavities were used in the visible and near-infrared. Experiments that followed focused on two mirror cavities and extended to the mid-infrared[2,3]. From the photon lifetime, the resonator mirror reflectivities are deduced, given the mirror spacing. With this approach, Herbelin et al.[1] were able to determine mirror reflectivities with a precision ranging from 50 to 5000 parts per million (ppm). This represents a sensitivity that is on the order of 2 orders of magnitude lower than the current pulsed CRLAS approach. To understand the reasons for this difference we shall look more closely at their novel approach and trace the developments that have led to the current CRLAS technique.

A simplified two-mirror block diagram of the CAPS experiment is shown in Figure 2. Continuous wave (cw) laser light is passed through an electro-optical birefringent modulator, producing a time-varying linearly polarized beam that is modulated as

$$\sin^2(2\pi ft \pm \Phi) \tag{1}$$

where f is the modulation frequency and Φ is the initial phase shift, usually set equal to 0. The modulated light is then coupled into the resonator through mirror M1 and detected after exiting the resonator outside mirror M2, where it is now shifted in phase by an amount α. This phase shift is related to the photon lifetime in the resonator via[1]

$$\tan \alpha = 4\pi f\tau \tag{2}$$

where the photon lifetime (τ) corresponds to a fixed number (n) of round-trip passes inside the resonator

$$\tau = nt' = \frac{2Ln}{c} \tag{3}$$

where t' is the time required for the photon to complete one round trip ($2L/c$). The number of round trips (n) made by the photon for a two-mirror resonator with reflectivities R_1 and R_2 (for cases where $R \approx 1$) is given by

$$n = R_1R_2/2(1 - R_1R_2) \tag{4}$$

Therefore,

$$\tan \alpha = 4\pi Lf(R_1R_2)/c(1 - R_1R_2) \tag{5}$$

If R_1 is known, R_2 can be determined from the above expression by measuring the phase shift α. Similarly, molecular absorption A (fractional absorption per pass) between the two mirrors can be incorporated with eq 5 (for $A \ll 1$):

$$\tan \alpha = 4\pi Lf(R_1(1 - A)^2R_2)/c(1 - R_1(1 - A)^2R_2 \tag{6}$$

A more complete derivation of the above expressions can be found in refs 1−3.

In practice, the phase shift can be determined with various detection arrangements, although it can most efficiently be obtained by directly measuring tan α with a two channel lock-in amplifier in the following manner: first, the modulator is placed outside of mirror M2 and both channels of the two channel lock-in are adjusted in phase to null out signals on both channels A and B. Next, channel B is shifted by 90° and the modulator is placed before mirror M1. In this arrangement, channel A is directly proportional to sin α and channel B is proportional to cos α. With the use of a ratiometer, $A/B = \tan \alpha$ can be obtained directly. A plot of tan α versus L for different resonator lengths or tan α vs f for various modulation frequencies provides a means of determining either the unknown reflectivities or the molecular absorption A.

Table 1. CAPS Technique Sensitivity (dR/R) as a Function of Mirror Reflectivity and Phase Angle Measurement Precision[a]

$R_1 = R_2 = R$	R^2	dR/R for $\delta\alpha = 5°$	dR/R for $\delta\alpha = 2.5°$	dR/R for $\delta\alpha = 1°$
0.999	0.998	2.4×10^{-4}	1.6×10^{-4}	7.0×10^{-5}
0.9995	0.999	1.5×10^{-4}	9.1×10^{-5}	3.3×10^{-5}
0.999 95	0.9999	1.6×10^{-5}	8.8×10^{-6}	3.5×10^{-6}
0.999 975	0.999 95	8.0×10^{-6}	4.2×10^{-6}	1.5×10^{-6}

[a] Typical reported experimental phase angle uncertainties were ~5°.

From the above description, the factors that determine the CAPS sensitivity become evident. Uncertainties in the phase shift, modulation frequency, and cavity length primarily dictate the achievable sensitivity. Uncertainties in the modulation frequency are typically very small (for the 10−20 kHz frequencies used) and can be significantly reduced by taking measurements at different frequencies and fitting the points to a straight line. Because the measurements were recorded on the order of 0.1 s time scales, fluctuations in the cavity length due to thermal drift and acoustic vibrations are averaged out and also lead to a small correction in the calculated reflectivity (or absorption). The limiting factor in attaining high sensitivity in the CAPS technique was due to the fluctuations in and the ability to measure the phase angle itself, with uncertainties on the order of 5−10° being reported.[1−3] These phase fluctuations were primarily associated with the erratic longitudinal mode coupling that occurred between the laser and resonator cavities during the measurement of the phase angle.[3] In this case, the measurement represents a large number of integrated, averaged mode matches between the cw input laser and cavity. These dynamic mode matches occur as a function of laser wavelength, line width, and mode quality coupled to the cavity mode spacing, line width, and stability. A discussion of the difficulties encountered due to dynamic mode matching in the CAPS technique can be found in refs 1−3, but it is currently sufficient to recognize that both phase angle uncertainty and mirror reflectivity combine to set an upper limit on the experimentally achievable sensitivity. To illustrate this point, consider the error in determining a reflectivity (i.e., $\delta R/R$) for mirrors of increasing reflectivity as a function of uncertainty in the phase angle about the value $\alpha = 45°$ (the situation gets worse for larger or smaller values of α). These data are given in Table 1 for values of R ranging from $R = R_1R_2 = 0.999$ to 0.99995. Due to the nature of the denominator in eq 5, small increases in the value of R lead to large gains in sensitivity, while decreases in phase angle uncertainty in this case scale almost linearly with sensitivity, as shown in Table 1. If it were possible to accurately determine the phase shift to within 1° with a set of mirrors with $R_1 = R_2 =$ 99.9975%, one could achieve an ultimate absorption sensitivity of roughly 2 ppm. The dependence of the CAPS technique upon the phase angle measurement introduced a significant experimental barrier to achieving higher sensitivity. Further development of this method will require either better stabilization of the cavity or total spoiling of the mode structure in addition to an increased precision in the phase angle measurement, which should be feasible with current technology.

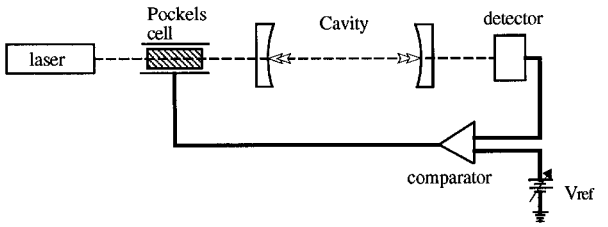

Figure 3. Mirror reflectometer of Anderson et al.: Instead of measuring the phase shift, the intensity decay of the cavity is measured after the light is quickly shut off with a Pockels cell. Ideally, the modes established in the cavity then undergo a first-order exponential decay.

The next major step in the development of the cavity ringdown technique was made by Anderson, Frisch, and Masser in 1983[4] and addressed the experimental difficulties associated with the CAPS method. Instead of inferring the cavity transmission from the measured phase shift, Anderson et al. directly measured the photon lifetime in the resonator by monitoring the *intensity decay* that occurred when the cw input laser was shut off with a fast optical switch. A diagram of their apparatus is shown in Figure 3.

In practice, cw laser light was injected into the cavity, and the transient buildup of energy in the cavity modes was monitored at the output mirror with a fast detector. When the cavity output intensity reached a specified threshold level (via the comparator), the Pockels cell was switched off and the transient response or "ringdown" of the cavity was monitored with an oscilloscope. In this fashion, problems arising from spurious mode-matching between the laser and cavity axial modes were greatly reduced, since the cavity was allowed to approach a more or less steady state.

If the switching time of the Pockels cell is on the order of one cavity roundtrip time, the cavity decays exponentially according to the first-order expression

$$I(t) = I_o e^{-t/\tau} \tag{7}$$

where τ is the "ringdown time" of the cavity (time when $I = I_o/e$). The ringdown time is related to the mirror reflectivity (for $R \approx 1$) via

$$\tau = \frac{L}{c}\left(\frac{\sqrt{R}}{1-\sqrt{R}}\right) \tag{8}$$

where L is the mirror separation, c is the speed of light, and $R = R_1R_2$ is the reflectance for a two-mirror configuration. A more detailed derivation of the above expressions can be found in ref 4.

In contrast to the CAPS method, the measured quantities in the Anderson et al.[4] technique are cavity length and decay time, and it is this difference that allowed a higher level of sensitivity to be achieved. This resulted from both the relaxed constraint on the decay time determination as well as the ease with which it was measured. With the use of fast detectors and electronics, the ringdown time of the cavity was measured with nanosecond precision. With this arrangement, Anderson et al. reported a sensitivity

Table 2. Sensitivity of the Mirror Reflectometer of Anderson et al. for Different Mirror Reflectivities[a]

R	no. of passes to $I = I_0e^{-1}$	dR/R for $\delta\tau/\tau = 1\%$	dR/R for $\delta\tau/\tau = 2\%$	dR/R for $\delta\tau/\tau = 3\%$	dR/R for $\delta\tau/\tau = 10\%$
0.9950	100	$\pm 5.05 \times 10^{-5}$	$\pm 1.02 \times 10^{-4}$	$\pm 1.5 \times 10^{-4}$	$\pm 5.5 \times 10^{-4}$
0.9990	500	1.01×10^{-5}	2.04×10^{-5}	3.0×10^{-5}	1.1×10^{-4}
0.9995	1000	5.05×10^{-5}	1.02×10^{-5}	1.5×10^{-5}	5.5×10^{-5}
0.9999	5000	1.01×10^{-6}	2.04×10^{-6}	3.0×10^{-6}	1.1×10^{-5}
0.999 95	10 000	5.05×10^{-7}	1.02×10^{-6}	1.5×10^{-6}	5.5×10^{-6}
0.999 99	50 000	1.01×10^{-7}	2.04×10^{-7}	3.0×10^{-7}	1.1×10^{-6}

[a] The sensitivity (dR/R) scales exponentially with the mirror reflectivity and linearly with the decay time precision. These data are also applicable to current pulsed CRLAS experiments.

of approximately 5 ppm per pass, representing at least 1 order of magnitude increase over the CAPS method.

Sensitivity limits for various reflectivities and decay time uncertainties are listed in Table 2 and illustrate the relaxed constraint on the decay time precision. These data should be compared to those for the CAPS method given in Table 1. For example, determination of the cavity decay time with a precision of 1% for a set of mirrors with $R = 99.99\%$ in the ringdown approach is more than 1 order of magnitude more sensitive than the CAPS method for a 5° uncertainty in the phase angle. Yet, this 1% error in the ringdown time determination is still orders of magnitude greater than the achievable limit, which will be discussed later. Although this new approach represented a significant improvement over the CAPS technique, the threshold triggering scheme employed also suffered from the dynamic mode matching that occurred between the cw laser and optical cavity. This condition prevented continuous scanning of the laser wavelength, since adjustment of the switching threshold, which could vary by orders of magnitude, would be required for each new wavelength. Although this could be achieved, it would likely be difficult to implement.

To address the drawbacks of the two previous techniques that resulted from the unpredictable mode matching between the cw laser and high finesse optical cavities, O'Keefe and Deacon[5] employed pulsed lasers for excitation of the cavity, thereby greatly simplifying the experimental arrangement. In doing so, the need for fast optical switches or threshold triggering schemes was eliminated, as the initial intensity of the cavity decay was no longer of any consequence. By using short pulse lasers with limited coherence lengths, interference in the cavity was essentially random; thus, continuous wavelength scanning was now feasible. In these initial visible experiments, the intensity decay was measured directly after the output mirror with a PMT, digitized, and sent to a computer for analysis in real time. With this new approach, a fractional absorption sensitivity of 1×10^{-6} was easily achieved. In the pulsed laser approach, derivation of the ringdown decay expression is greatly simplified, since the light pulse that is injected into the cavity can be effectively visualized as particle-like in nature. Because the amount of light that exits the resonator is directly proportional to the cavity transmissivity (T) and the intensity I of the trapped pulse, the time derivative of the output pulse is simply

$$dI/dt = -ITc/2L \tag{9}$$

where L is the mirror separation and c is the speed of light. The solution to this equation is

$$I = I_0e^{-Ttc/2L} \tag{10}$$

This expression can be rearranged to yield the total round trip loss (Γ) experienced by the light pulse while traversing the resonator

$$\Gamma = 1 - e^{-2L/c\tau} \tag{11}$$

where τ is the $1/e$ decay (ringdown) time. A plot of cavity loss versus wavelength allows one to extract either the transmission curve for the two mirrors or the absorption spectrum for a sample located between them. As in the experiment of Anderson et al., the sensitivity of the technique is limited by the mirror reflectivities and the precision in the determination of the decay time, with the associated values for various cavity configurations also given by Table 2.

The high sensitivity of the pulsed "ringdown" method was explicitly demonstrated by O'Keefe and Deacon in 1988 by measuring the doubly forbidden $^1\Sigma_g - X^3\Sigma_g$ visible bands of O_2 in a static gas cell and found to be roughly 1 ppm (fractional absorption) per pass.[5] This represented roughly a factor of 5 improvement over the apparatus of Anderson et al. Current state-of-the-art cavity ringdown experiments have exhibited slightly higher levels of sensitivity. Since its initial development, the pulsed "cavity ringdown" method has been successfully employed in a number of spectroscopic studies and further developed for a variety of other novel applications.

CRLAS Applications

In the last decade, numerous researchers have employed and developed the cavity ringdown technique for various purposes, including the spectroscopic study of molecules and clusters. In this section, we summarize this development. Although an effort has been made to cover this work comprehensively, the rapidly evolving nature of the field guarantees that this discussion will be incomplete by the time of printing of this paper.

Shortly after the initial gas cell measurements of O'Keefe et al., CRLAS was developed for molecular beam spectroscopy by O'Keefe and Saykally and coworkers at Berkeley.[6] The apparatus employed was a hybrid of the "cavity lossmeter" of O'Keefe and Deacon and the molecular beam apparatus of the Saykally group that had been used primarily for the study of laser-vaporized carbon clusters.[7] In this work, vibronic spectra were obtained for a variety of transition metal clusters, including the copper dimer

and trimer systems.[6] In this initial application of CRLAS to the study of laser-generated molecular beams, several potential difficulties were addressed. The transient nature of the molecular beam, high plasma density, and large shot to shot fluctuations typical of laser vaporization sources were of primary concern. Although these factors did in fact limit the attainable sensitivity to 5−10 ppm (fractional absorption) per pass, this initial work demonstrated the suitability of the ringdown technique for molecular beam spectroscopy and underscored the potential of the method for other applications. These molecular beam studies have since been extended to include a number of metal cluster and metal silicide studies. Results from some of the molecular beam studies will be summarized later in this review.

The next application of the ringdown technique was demonstrated in 1991 by Benard and Winker,[8] who utilized a novel variation of the approach to detect either the optical gain or loss in a laser-induced chemical reactor. In that experiment, the active volume of a CO_2 laser pumped-flow reactor was situated at the center of a confocal ringdown cavity ($L = 50$ cm), at right angles to both the gas flow and CO_2 laser pump axes. The ringdown measurement was performed with an excimer-pumped dye system and detected with a fast photodiode and oscilloscope at the exit mirror. A delay between the photolysis laser and ringdown probe laser facilitated buildup of a population inversion in BiF before spectral interrogation.

In 1993, Yu and Lin[9] reported on the first development of the ringdown technique for kinetics studies. In that work, phenyl radical was generated by laser photolysis of nitrobenzene, followed by spectral interrogation with the pulsed cavity ringdown technique. The exponential decay of the photolyzed product was accounted for by replacing the absorption term in the ringdown expression with an absorption (concentration) exponential decay factor given by $A = A_o \exp(-k't')$, where k' is the pseudo-first-order decay constant of phenyl and t' is the time after firing of the photolysis laser. The absolute values of the second-order rate constants were then determined from the slopes of the linear k' vs concentration plots. The validity of this approach stemmed largely from the fact that the lifetime of the photolyzed product (5−10 ms) was orders of magnitude longer than the associated ringdown times (ca. 25 μs). Lin and coworkers have tested the accuracy of the cavity ringdown approach described above for kinetics studies by measuring the rate constant of the $NH_2 + NO$ reaction via the NH_2 absorption spectrum at 537 nm.[10] These studies have since been extended to include the $C_6H_5 + NO \rightarrow C_6H_5NO$ reaction,[9] wherein the C_6H_5 absorption band at 505 nm was monitored, the $C_6H_5 + CCl_4$ reaction (in the presence of O_2) wherein the $C_6H_5O_2$ product was monitored via its 510 nm absorption band,[11] and further experiments of the $NH_2 + NO$ reaction, again monitored via the NH_2 absorption at 537 nm.[12] The mirrors used in these studies had typical reflectivities of 99.99%.

The experiments of Lin and co-workers demonstrated the feasibility of using the ringdown method for kinetics studies. In theory, this approach could be extended to faster kinetics processes than those explored above, as long as the chemical dynamics are significantly slower than the fitted time region of the ringdown decay. This same application of CRLAS for kinetics studies has also been recently implemented by Zhu and Johnston[13] for studying the reaction of vinoxy radical with molecular oxygen.

Romanini and Lehmann[14,15] have used CRLAS to obtain overtone spectra of HCN in static gas cells, in search of chaotic behavior in highly excited vibrational states. In these experiments, the CRLAS spectral intensities for the HCN (105) overtone were found to be different from those obtained in photoacoustic studies, but were in agreement with ab initio calculations. In these experiments, a novel boxcar scheme was utilized to measure the ringdown signal, and a Brillouin cell was located before the cavity to reject the input laser ASE, which in some cases could otherwise lead to a reduction in the extracted absorption intensities. This point will be further addressed in the discussion of laser bandwidth considerations presented later in this article.

Meijer et al.[16] have extended CRLAS into the UV in a study of the 300 nm band of OH obtained in a small Bunsen burner flame. Absorption spectra were obtained with a multimode dye laser (~1.2 GHz bandwidth) and used to calculate the temperature of an atmospheric pressure methane−air flame. Mirror reflectivities used in that work were ca. 99.5%, resulting in very fast decay times and subsequent lower sensitivity. In the case of flame spectroscopy, small ringdown cavities combined with small burner dimensions helped to minimize thermal lensing effects (e.g., beam walking), which can significantly degrade cavity alignment. These effects are more severe at shorter wavelengths since they are dominated by nonresonant processes that typically scale exponentially with frequency.

In this same study, experiments were performed wherein narrow band (~5 MHz) cw laser light was coupled into cavities of on- and off-confocal geometry, which revealed the transverse and longitudinal mode structure of the ringdown cavity. The researchers then measured the visible absorption spectrum of iodine with a pulsed laser and nonconfocal cavity geometry and interpreted the absence of distorted or missing spectral features as being explicitly due to the near-continuous mode spectrum of the cavity. This extrapolation of cw experiments to explain the results obtained with the multimode pulsed laser raises questions as to the role of interference effects in pulsed ringdown spectroscopy, which in most cases will be negligible. Although this topic has been raised frequently in the literature, no experimental evidence has been presented to date that supports the aforementioned anomalous distortion of spectral intensities due to interference phenomena in pulsed ringdown experiments. This topic will be explored in more detail later in this review.

Meijer and co-workers have since utilized the ringdown method for the detection of trace species in the gas phase[17] and have also used CRLAS absorption measurements in a static gas cell to determine the absolute transition strength of the 206 nm Cameron band of CO.[18] In this study, a fractional

absorption sensitivity of 50 ppm was demonstrated even though relatively low mirror reflectivities (R = 98.45%) were used. Boogaarts and Meijer[19] have also recently used ringdown spectroscopy in conjunction with a mass spectrometer and laser desorption apparatus to estimate the number density of desorbed diphenylamine molecules.

Zalicki et al.[20] have employed CRLAS to detect the methyl radical in a hot filament flow reactor via the 216 nm band. The spatial dependence of the methyl concentration in the vicinity of the filament was derived from the associated intensity of the absorption spectrum. In this work, an absorption sensitivity of 20 ppm was reported, and the broad vibronic band spectra obtained exhibited a signal to noise ratio roughly four times better than that of previous conventional absorption measurements and comparable to that obtained in atmospheric pressure flames with the method of degenerate four wave mixing (DFWM) recently reported by Farrow and co-workers.[21] These flow reactor studies are currently being employed to gain insight into the chemistry of diamond film growth.

Scherer et al.[22] have recently extended CRLAS into the 1.6 and 3.3 μm regions of the mid-infrared. In that work, a single mode optical parametric oscillator (OPO) laser system was employed to obtain Doppler limited spectra in static gas cells. In these studies, the high mirror reflectivities (R > 99.95%) allowed a sensitivity of better than 3 ppm (fractional absorption per pass) to be obtained. Comparison of IR-CRLAS overtone spectra of acetylene obtained in the 1.6 μm region with state-of-the-art photoacoustic data demonstrated nearly 1 order of magnitude greater sensitivity for IR-CRLAS. IR-CRLAS has also been recently implemented by Scherer et al.[23] as a nonintrusive diagnostic of chemical species in low pressure flames in the 1.6−4 μm region.[24] In this work, sensitivity, spectral congestion in high-temperature hydrocarbon flame environments, and the ability to operate in moderately sooting flames was explored. Additionally, comparison of the IR-CRLAS flame spectra to those obtained by other infrared methods demonstrated at least 1 order of magnitude greater sensitivity for IR-CRLAS. CRLAS has also been recently used by Scherer and Rakestraw to determine the HCO radical concentration in a low pressure flame.[25]

Paul et al.[26] have recently utilized IR-CRLAS to study vibrational bands of water clusters in the mid-infrared, obtaining vibrationally resolved spectra for jet-cooled $(H2O)_n$ clusters up to n = 5. In this work, a dye-laser pumped multipass hydrogen Raman shifter was employed to generate tunable infrared laser light to probe water clusters in the mid infrared. Using this same apparatus, spectra have also recently been obtained for the uracil, thymine, and adenine monomers and dimers, consisting of the N−H stretching modes of the associated species.

Engeln and Meijer[27] have recently reported the combination of visible CRLAS with a Fourier transform (FT) spectrometer. In this demonstration, broadband laser light is first coupled into the ringdown cavity and then directed into a commercial FT instrument. Obtaining an interferogram in combination with the intensity decay of the resonator allows a spectrum to be obtained with comparable sensitivity to that of currently available FT systems that employ multipass configurations. The challenge in employing this approach for spectroscopic studies currently lies in the effective scanning speed, which is currently slower than the conventional CRLAS approach wherein the input laser is scanned. With further development, however, this approach will likely have a variety of valuable and unique applications.

Recently, Giles et al.[28] have used CRLAS to obtain the doubly forbidden $^3\Delta$-$X^1\Sigma$ vibronic transitions in diacetylene in the 396−342 nm region, and Pearson et al.[29] have employed CRLAS for the study of the J-dependent line broadening in the A−X system of HNO. All of these studies have clearly established the widespread applicability of CRLAS for sensitive spectroscopic measurements and foreshadow the increased use of this rapidly developing technique. In the following sections, we review a variety of theoretical and experimental issues that are fundamental to all of the above applications of CRLAS.

III. CRLAS Sensitivity and Fundamentals

In this section we address the variables that influence the attainable sensitivity in CRLAS. Examples are presented that highlight the fundamental limitations associated with a given experimental configuration. Unlike techniques that are typically limited by simple photon- or ion-counting statistics, the sensitivity in CRLAS can be dictated by a complex interplay of many variables.

In CRLAS, as with other absorption methods, sensitivity is most generally discussed in terms of the minimum detectable fractional absorption *per pass*, since this allows an unambiguous definition for a specified number density and absorption cross section. We explicitly avoid the use of effective absorption path length values (derived from the number of passes in the decay time) or sensitivity limits in terms of inverse path length since in the former this value changes with the strength of the absorber and in the latter it is specific only for a given molecule with a fixed number density and absorption cross section. It therefore follows that if we do choose to specify the effective absorption path length as that equal to the number of passes that occur during the decay time, the fractional absorption uncertainty is then equal to the decay time uncertainty, and not the smaller absorption per pass value used throughout this paper. In either case, the fundamental limitation of the sensitivity of CRLAS is determined by the accuracy of the ringdown time measurement. As mirror reflectivity increases, the fractional uncertainty in the decay time will generally decrease, which subsequently leads to a higher sensitivity limit. This fact makes it essential to specify mirror reflectivities to assess the sensitivity limit of a CRLAS experiment. Although the theoretical limit is typically not achieved in most CRLAS experiments, higher mirror reflectivities offer the simplest means of routinely achieving ppm sensitivity levels without a great deal of effort. This point underscores the desirability and high priority of obtaining mirrors

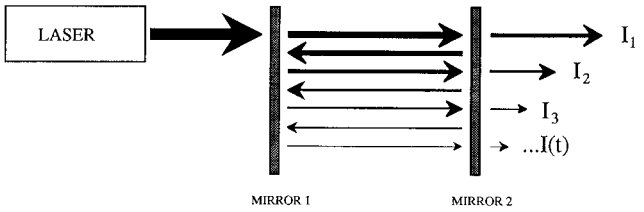

Figure 4. First-order picture of the cavity decay. Because the laser light is incoherent over the dimensions of the cavity, the light acts like a particle as it bounces back and forth between the mirrors. The intensity monitored at the output mirror is therefore simply a function of the single pass transmission coefficient of the cavity.

with the highest possible R value. For a given set of mirrors, cavity length, laser properties, and detectors are the primary variables that dictate the experimentally achievable sensitivity.

First-Order Considerations

A convenient starting point for the discussion of CRLAS sensitivity is the ideal model used in derivation of the first-order exponential expression for the cavity decay time. In this model, the spatial length of the laser pulse injected into the cavity is much shorter than the cavity round trip length, leading to discrete pulses being transmitted through the exit mirror of the cavity with each round trip. In this limit, interference effects are not important. Figure 4 illustrates this situation, where the multiple reflections that occur in the cavity during the decay are represented by displaced arrows. In this picture, the intensity measured at the photomultiplier will be a series of pulses of regularly decreasing intensity spaced in time by $2L/c$ (see also Figure 1). The peak intensities of these discrete pulses fit to a first-order exponential decay, from which the cavity losses are determined. In this case, the ultimate sensitivity will depend explicitly on the ratio of the uncertainty in the number of round trips passes of the light pulse to the total number of round trips that occur during the actual *measurement* of the ring down time. For example, consider a cavity comprised of mirrors having reflectivities $R_1 = R_2 = 99.995\%$ that are spaced 0.5 m apart. In this case, one would measure a $(1/e)$ decay time of 33 μs, during which time the light pulse would make 10 000 round trips, as shown earlier in Table 2. In this case, determination of the time constant to within a single round trip (1 part in 10 000) would translate into a spectrometer absorption sensitivity of 5 parts per billion. If the individual pulses are well separated and it is possible to discriminate the individual features of each pulse, the cavity decay time can be determined with a precision greater than the transit time of the light pulse across the cavity, that would subsequently lead to increased sensitivity. This would most easily be achieved by assuring the length of the laser pulse ($\sim$1 ft/ns) is less than the round trip length of the cavity; otherwise, the ability to discriminate individual light pulses would likely be lost. For example, an excimer pumped dye laser with a 15 ns (FWHM) pulse would undergo ca. 5 round trips in the same 0.5 m resonator in the duration of the laser pulse. In this case, the ringdown decay would at best exhibit periodic fluctuations on the round-trip time. While points on the decay spaced in time by $2L/c$ still fit to a simple exponential, and the envelope of these fluctuations should decay exponentially, when averaged over the round-trip time these fluctuations will produce steps rather than a smooth decay. If we assume that this nonexponential nature will limit the determination of the time constant to a single round trip, then the above sensitivity of 5 ppb fractional absorption per pass is realized.

In the discussion of absorption sensitivity, it is important to realize that in CRLAS, as the absorption strength increases, the associated precision of the decay time measurement is reduced. For example, a cavity with a base-line loss of 100 ppm with a 10 ppm absorber is capable of determining the absorption to a precision of 1 ppm for a decay time precision of 1%, while a 400 ppm absorber in the same cavity is only accurate to within 5 ppm for the same 1% decay time precision. In essence, the CRLAS method becomes less accurate as the absorption intensity increases, since the decay time is shorter for larger absorption. In this regard, CRLAS possesses a somewhat limited dynamic range, which is severely reduced as mirror reflectivity decreases. Typically, CRLAS is unsuitable for measuring fractional absorption of greater than a few percent and is therefore complimentary to other methods, such as Fourier transform spectroscopy, that are capable of accurately measuring absorption that approaches 100%. Experimentally, the absolute absorption intensity is further limited by the inability to completely separate the total transmission of the cavity plus sample from the transmission of the empty cavity. In effect, by fitting the decay to an exponential expression, we are distributing the losses in the cavity over the entire cavity length, and we do not have the ability to actually spatially resolve the discrete regions of loss. This is usually a minor limitation, however.

From this discussion, it is clear that extremely high levels of sensitivity can be reached (in theory) with the CRLAS technique. In practice, however, there are many factors that limit the experimentally achievable sensitivity. Contributions from uncertainties in data acquisition and analysis, laser and detector noise, cavity alignment, and mode competition can combine to degrade technique sensitivity by orders of magnitude. In the following sections we discuss several of these points in greater detail.

Data Acquisition

One of the first concerns in the design of the Berkeley CRLAS apparatus was the choice of waveform recording instrumentation. Our decision to use a digitization format over analog methods was based on several practical considerations. Digitization of the decay allows fast, accurate acquisition of the entire decay and provides a versatile format for data manipulation such as signal averaging. Additionally, it allows the ringdown signal to be quantitatively monitored during the alignment procedure. Although this point may appear trivial, in fact, it is extremely critical, since multiexponential decays are not typically discernible by visually monitoring an oscilloscope trace. In our case, a single decay event is fit in two different regions, and the associated

decay time constants for the two regions are compared. This allows the cavity to be tuned until the two fitted decay times are identical, thus ensuring that the cavity is undergoing a single exponential decay. This criterion is essential for extracting accurate relative absorption intensities and highlights the advantage of a digital format over analog methods, such as comparators or boxcar schemes. Some groups have employed boxcar averaging schemes that effectively use two points in the decay to measure the ringdown time. The boxcars in this case can, in principle, be scanned in time to check for single exponential quality during initial alignment, but this approach would be cumbersome in wavelength scanning applications. In the event that the boxcars are not scanned in time, the decay is effectively fit with only two points, leading to a more stringent requirement on the precision of these points, as opposed to the digitization format wherein the decay is fit using hundreds or thousands of points in a least-squares fitting routine.

In the case of a digitization format, two quantities must be considered: sampling rate and analog-to-digital conversion resolution. These quantities can be tailored to a specific cavity geometry and detection scheme to give the largest number of points with the highest degree of precision. Modern transient digitizers typically possess a clock accuracy on the order of picoseconds. Therefore, the sampling rate generally need only be considered in terms of the limitation that it places on the number of points that will be used in the fit. The A−D conversion, on the other hand, is critical because it will limit the precision of these points. For example, a 100 MHz 8-bit digitizer used in conjunction with a 0.5 m resonator with a 33 μs ringdown time would lead to a sampling capability of several thousand points in time but would be limited by the A−D resolution of only 1 part in 256. In contrast, a 20 MHz 12-bit unit would be limited to ca. 600 points in time but with a precision in intensity of 1 part in 4096, a factor of 16 better than an 8-bit unit. Empirically, we have found that only one-fourth the number of laser shots are needed with the 12-bit unit to achieve the same level of sensitivity as with the 8-bit unit, as expected from simple statistical arguments.

Shot Noise

Although the extent of laser and detector noise will vary according to the specific equipment, the manner in which these noise sources contribute to CRLAS sensitivity is straightforward and has been explored by several researchers (see, e.g., refs 14 and 17). The contribution from laser photon noise (shot noise) is treated by comparing noise in the detection apparatus with the theoretical photon-counting limit of the light that exits the cavity and ascertaining how this noise contributes to the determination of the cavity decay time constant. Consider, for example, the case where a typical excimer-pumped dye laser that produces a 10 mJ, 15 ns pulse of narrowband light at 500 nm is injected into a 0.5 m ringdown cavity and is detected with a fast (2 ns) photomultiplier. In this case, a pulse consisting of ca. 10^{16} photons is produced, with $\sim 3 \times 10^7$ photons reaching the detector in the first pass through the cavity (for $R = 99.995\%$). At the cavity ringdown time, ca. 1×10^7 photons strike the detector in 15 ns, leading to a shot noise limit (which scales with the square root of the number of photons) of ca. 3×10^{-3} in the last pulse as it exits the cavity. In the worst case scenario, this could lead to an uncertainty in the ringdown time of at most 3×10^{-4}, which in turn translates into a spectrometer sensitivity of ca. 2×10^{-8}. Because the ringdown time measurement typically consists of thousands of such pulses, this small uncertainty in the *amplitude* of a single pulse is insignificant to the overall precision of the ringdown *time* determination, as long as a least-squares fitting program can be implemented. In the digitization format, random intensity fluctuations such as those from shot noise would typically average out and contribute very little to the overall precision in determining the decay time constant. Therefore, the shot noise limited sensitivity value of 2×10^{-8} described above can be up to several orders of magnitude worse than the actual value attainable. From this example, it is clear that when statistical fitting methods are employed, shot noise is the limiting factor only in the case of extremely low (submicrojoule) laser fluence.

Laser Bandwidth and Multiexponential Decays

So far, we have not considered in detail the frequency spectrum of the laser light trapped in the cavity. In the event that CRLAS is implemented for quantitative analysis of spectral intensities, the laser bandwidth with respect to the absorption line width must be considered, as is the case in conventional absorption spectroscopy (i.e., applicability of Beer's law). However, several phenomena that are unique to CRLAS can occur that can result in non-exponential cavity decays and subsequent distortion of the spectral intensities. Some of these phenomena have been discussed in previous studies and are outlined in this section.

For the case of an empty cavity, the ringdown time is dictated by the frequency-dependent reflectivity of the mirror coatings, and there will always exist a range of decay times for a given bandwidth. The more broadband the laser light, the larger this range of decay times, and hence the lower the ultimate sensitivity. If each frequency of the input bandwidth is not equally attenuated with each pass, accurate values for the cavity loss are not obtained from fits to a single exponential (eq 11) Similarly, when a sample is placed into the cavity, accurate absorption intensities are not obtained.

In the case of molecular absorption, we must consider the specific interaction of the input laser spectral content with the absorbing species. Additionally, in some cases, we must also consider the interaction of the molecule with the successive pulses of the circulating light. We will consider the latter case in more detail later in the discussion of interference effects. In the former, consider the case of molecular absorption where the line width of the molecule is less than that of the laser light that is coupled into the cavity. As the laser pulse circulates in the cavity, only frequency components resonant

with the molecular transition are absorbed. This effect leads to decays that can deviate significantly from a single exponential and results in under calculation of the absorption intensity. If the light exiting the cavity were dispersed into its various frequency components, different decay times would be measured for the resonant and nonresonant components, with subsequent increased absorption for the resonant components. This point has also been discussed previously by other researchers, including Meijer and co-workers[16,17] and Zalicki and Zare.[30] Hodges et al.[31] have experimentally demonstrated that in cases where the laser light consists of multiple modes and is broader than the line width of the absorber, its frequency spectrum must be explicitly included to extract accurate absolute absorption intensities.

Amplified spontaneous emission (ASE) can similarly degrade sensitivity, since the resultant broadband light can in some instances constitute a significant fraction of the light trapped inside the cavity. Romanini and Lehmann[15] have in one study utilized a Brillouin cell to remove ASE from their input laser. For most state-of-the-art lasers, however, ASE only constitutes a small fraction (typically $\sim 10^{-3}$) of the total laser light and, therefore, presents no significant problem.

One extreme case that deserves attention is the case wherein narrow absorption is strong enough to effectively burn a hole into the frequency spectrum of the input laser light. In this case, the total intensity-monitored decay (assuming no wavelength separating element is employed in front of the detector) would have primarily two characteristic decay times; one fast decay that included the absorption and a second decay dominated by the nonresonant frequencies. We can easily estimate the absorption intensity that would be required to easily see this effect. For a cavity constructed of 99.995% reflective mirrors, only $(1 - R)$, or 0.005%, of the light is transmitted with each pass. Therefore, the number of round trips (x) to the $1/e$ cavity decay time is found by solving

$$1/e = R^{2x} \tag{12}$$

which is solved by taking the natural log of both sides to yield

$$2x = -(\ln 0.99995)^{-1} \tag{13}$$

In this case, the laser light will undergo 10 000 round trip passes to its $1/e$ time. If an absorber of 1000 ppm (fractional absorption per pass) is placed in between the mirrors, the number of round trip passes to $1/e$ for the resonant frequency component will be reduced to 475. If we define the hole-burning point to be when only 1% of the resonant light is left in the cavity, then the number of passes the laser will make through the sample with mirrors of reflectivity R before the resonant frequency component is burned out, for an absorption A, is found with the expression

$$0.01 = -[R(1 - A)]^{2x} \tag{14}$$

In the above example, the cavity intensity decay is dominated by the non-resonant component after 2200 passes. This point has important consequences for the extraction of relative absorption intensities when both strong and weak absorption is measured with laser light that is broader than the absorption line width. In this case, the ringdown should be fit only in the temporal region where maximum attenuation occurs (i.e., the earliest part of the decay). We have encountered this effect many times, especially when strong absorption features (e.g. bandheads) are measured. The overall result is an apparent decrease in the relative absorption strength for the stronger absorbers, as well as a reduced absorption dynamic range.

Interference Effects in CRLAS

The topic of interference effects in ringdown spectroscopy spans a variety of issues that in this section we will divide into two subtopics. In the first, we will focus on the transmission variation or "fringe contrast" of the cavity that results when the laser pulse is longer than the mirror spacing, that in coherent limits is adequately described by Fabry−Perot theory. The challenge in this topic is to accurately predict this contrast as a function of the input laser properties and theoretical cavity mode structure. The topic of the response of empty optical cavities can be found in many texts, including Siegman,[32] and has been previously discussed by us[33] and others[34] for the specific case of CRLAS. In the second topic we will address the issue of coherence effects that can occur when an absorbing sample is placed in the cavity. This issue has been discussed for the specific case of CRLAS by Meijer and co-workers[16,17] and theoretically discussed by Zalicki and Zare[30] and recently by Lehmann and Romanini.[35] The challenge in this case is to accurately predict the net effect on the observed decay time of the cavity, since this is the only measured quantity in CRLAS. In some cases, this requires a discussion of phenomena such as Ramsey fringes and nonlinear absorption. In spite of the potential difficulties associated with either significant intensity transmission variation or the coherent phenomena described below, it is important to recognize that the above limits are generally easily avoided and do not constitute a significant barrier to researchers wishing to implement CRLAS. To date, no significant absorption anomalies have been reported in CRLAS studies that are attributable to the interference effects discussed below. Rather than attempt to comprehensively discuss all possible interference phenomena in ringdown spectroscopy in this review, we will only outline the associated issues, referring the reader to more detailed analyses and relevant experiments where appropriate.

The issue of the fringe contrast or frequency selective energy buildup in an empty cavity will first be treated in the coherent limit, followed by a discussion of the applicability of the results to the quasi-coherent regime. When the cavity is injected with light that overlaps with itself (traveling in the same direction) frequencies resonant with the cavity modes can be enhanced due to constructive interference while frequencies that are in between modes can

be attenuated due to destructive interference. The result in this coherent case is an effective spectral filtering of the injection laser input pulse. The energy buildup in this case is measured as a variation of the initial transmitted intensity at the output mirror of the cavity as the laser wavelength is scanned over the cavity free spectral range. This transmission or fringe contrast can become significant as the laser pulse length and coherence length increase with respect to the cavity dimensions. The ultimate sensitivity of the pulsed CRLAS method may in certain limits be hindered by the combination of the long coherence lengths that accompany high-resolution laser light and the high reflectivity of the resonator, which is required for high sensitivity. To predict the degree of contrast expected for a given configuration, the laser bandwidth (or coherence length) must be compared with the longitudinal and transverse mode spectrum of the cavity. Tailoring of the input light to mode match to a fewer number of cavity transverse modes as well as stabilization of the cavity will increase the resultant transmission contrast.

For optical cavities comprised of two identical spherical mirrors, the fundamental (or longitudinal) mode spacing ν_o of the cavity is given by $c/2L$, where L is the mirror spacing. Frequencies for the higher order transverse modes are calculated from the expression

$$\nu_{\mathrm{TEM}} = \nu_o[q + 1 + \pi^{-1}(m + n + 1)\cos^{-1}(1 - d/r)] \quad (15)$$

where q is the longitudinal mode index, m and n are the transverse mode indices, d is the distance between the mirrors, and r is the mirror radius of curvature.[36] For all but confocal or planar cavities, higher order transverse modes are shifted in frequency with respect to the fundamental longitudinal modes. In the case of confocal cavities, higher order transverse modes are degenerate, leading to an effective mode spacing of $c/4L$. The ability to excite higher order transverse modes depends explicitly on the cavity geometry and the input light characteristics and injection angle. Two limits are invoked in deriving the spatial extent and the stability of the cavity transverse modes: the infinite mirror limit[37] wherein the optic diameter is much larger than the input beam transverse dimension and the finite mirror or diffraction limit,[38] wherein the input beam is larger than the optic diameter. In the finite mirror limit, the stability or lifetime of a given transverse mode is dominated by the associated diffraction losses that are dependent on the Fresnel number and stability factor g ($g = 1 - d/r$) of the cavity (see, e.g., ref 36). The ability to preferentially build up energy in the cavity in a given longitudinal or transverse mode depends on all of the above factors.

The fringe contrast of an optical cavity is most simply determined in the limit described by Fabry–Perot theory,[40] where we assume that the light is monochromatic (or single mode) and therefore coherent with itself for any arbitrary pulse length. In this case, the number of cavity modes excited by the input light will be determined simply by the overlap of the injection laser with the cavity mode spectrum, assuming that diffraction losses are negligible (i.e., infinite mirror limit) and that the cavity is stable. In the following discussion, it is shown how an Airy function can be generated via the periodic addition of coherent light segments into the resonator. The motivation for this treatment is to mimic the case where the injected light is single mode and temporally longer than the round trip time of the cavity and to study what happens as the laser coherence length becomes shorter than the pulse length, i.e., no longer single mode.

If the length of the pulse is on the order of several cavity round trip lengths, we may partition the input pulse into lengths in those units. In this manner, the overlapping input pulse can be approximated by N pulses $E(t)$, applied at intervals of the cavity round trip time (T). Since the cavity finesse is extremely high, we will assume the amplitudes of the pulses will be essentially constant over several round trips. The intensity monitored at the output mirror as the laser is scanned over the modes of the cavity can be obtained by taking the Fourier transform of the field intensity inside the resonator in the time domain. For the case of two pulses injected into the cavity, the time variation of the electric field will be

$$E^{(2)}(t) = E(t) + E(t - T) \quad (16)$$

As long as the phase of the pulse is preserved over at least two round trips, the Fourier transform of this is given by

$$E(\omega) + \exp(-iT\omega)^*E(\omega) \quad (17)$$

which states that the time delayed pulse is identical to the nondelayed pulse, aside from a phase shift. The corresponding Fourier transform of the two-trip signal (normalized to unity) is

$$E^{(2)}(\omega) = (1/2)(1 + \exp(-iT\omega))^*E(\omega) = E(\omega)\cos(T\omega/2)\exp(-iT\omega/2) \quad (18)$$

with a corresponding intensity

$$I^{(2)}(\omega) = |E^{(2)}(\omega)|^2 = I(\omega)\cos^2(T\omega/2) \quad (19)$$

This signal is the same as the single period spectrum, except that it is modulated by a $\cos^2$ term, causing it to be unity at frequencies where $\omega = (2\pi q/T)$ and zero halfway in between (q = mode number). Hence, after only two round trips, the cavity mode structure has already become loosely defined. Extending this case to N successive repetitions of the signal $E(t)$ that are delayed by T yields

$$E^{\mathrm{N}}(t) = \sum_{n=0}^{N-1} E(t - nT) \quad (20)$$

the Fourier transform of which is

$$E^N(w) = \sum_{n=0}^{N-1} e^{-\mathrm{in}Tw}E(w) = \frac{1 - e^{-iTwN}}{1 - e^{-iTw}}E(w) \quad (21)$$

Therefore, the spectral power density is

$$I^N(w) = |E^N(w)|^2 = \frac{1 - \cos NTw}{1 - \cos Tw} I(w) \quad (22)$$

From this treatment,[40] it can be seen that the fixed time delay combined with the well-defined phase relationship between successive pulses gives rise to the transmission "fringes" of the cavity. As the number of round trips N is increased, the cavity fringes (or modes) will sharpen, with a width (FWHM) of $\Delta\omega_q = \omega_{ax}/N$, where ω_{ax} is the longitudinal mode spacing. For example, a 0.5 m cavity ($c/2L$ = 300 MHz for a planar cavity) with R = 99.995%, which is excited with a single mode laser pulse of ca. 5 m in length, would exhibit an associated transmission fringe width (FWHM) given by $\Delta\omega_q$ = 300 MHz/5 = 60 MHz. It is interesting to note that this 60 MHz cavity line width is simply the transform limit of the 5 m laser pulse. Deviations in the frequency-dependent cavity transmission predicted above, however, can occur due to several factors.

In the preceding analysis, the input laser light was approximated by successive pulses differing from each other by a constant phase factor, applied periodically at intervals of the cavity round trip time. The periodic application of these pulses subsequently assured that there existed a constant phase relationship among the different segments. The extrapolation of this model to the case of a single pulse of light that overlaps many times in the cavity is rigorous only for the case wherein the input laser light coherence length is equal to the pulse length, as, by definition, the coherence length of light is the distance over which there exists a phase relationship among different temporal segments of the light. If the laser pulse overlaps with itself such that the coherence length of the light is exceeded, the above partitioning of the light pulse into successive coherent segments is violated and the cavity fringe contrast is degraded.

The different regimes wherein the frequency specificity of the cavity may become a factor can best be illustrated by example. Consider the case of a 1200 MHz, 15 ns light pulse (common for commercially available pulsed dye lasers) and a 0.5 m cavity. The laser pulse would in this case overlap itself nearly five times, and the amplitude and phase of the pulse would vary on the time scale of the cavity round trip. In this case, the coherence length would constitute a small fraction of a single pass, and the previous analysis would break down as there is no longer a simple periodicity to $E(t)$ during the overlap period. The condition that the coherence length is less than the cavity dimensions can also be expressed as the condition that the laser bandwidth is greater than the cavity longitudinal mode spacing.

As another example, consider a 0.25 m cavity that is injected with a 15 ns pulse of laser light that possesses a coherence length that is several times the cavity round trip length, such as that from a cw-seeded, pulse amplified dye laser. In this case the pulse length is also five times the cavity round trip length, but in contrast to the above case, we would expect pronounced interference effects, due to the preserved coherence of the light pulse during overlap. Although in this event there can exist a significant difference in the initial intensity (i.e., on and off the cavity mode) or in some cases a modulation of the decay (due to mode competition), it is important to point out that the characteristic decay time of the cavity is essentially unchanged. It is also important to note that the cavity can never be excited to the extent that *no* light exits it per round trip (i.e., infinite contrast), since this solution is only mathematically realized for the specific case of exactly two overlaps in the cavity. Even in this case, however, the result is a near 100% modulation depth of the decay for each round trip period, while the overall envelope of the decay is still exponential.

The above-discussed modulation of the output can be eliminated altogether by choosing a cavity geometry such that the coherence time of the injection laser is less than the characteristic periodicity of the cavity. This condition is guaranteed when either the pulse coherence length is much less than the cavity length, or when the cavity is mode matched to a large number of transverse modes (for nondegenerate cavity mode configurations).

A final note in this discussion of transmission or fringe contrast is the role of the cavity mechanical stability, which typically limits the effective finesse (free spectral range/mode width) of the cavity and can altogether wash out the cavity mode structure. Mechanical vibrations, in the case of an unstabilized resonator, will decrease the extent of interference (standing waves) in the cavity when the mirrors undergo motions that significantly dephase the light. This dephasing of the light occurs when the mirrors move a distance on the order of the wavelength of the input light on a time scale of the round trip transit time of the cavity. For example, a 0.5 m cavity with a round trip time of ca. 3 ns would not possess a discrete mode spectrum during the decay time if subjected to vibrations on the order of hundreds of MHz. Vibrations on the order of acoustic frequencies (e.g., 10 kHz), on the other hand, would not significantly effect the cavity mode structure. Similarly, variations in the number or intensity distribution of the injection laser modes that occur as the laser is scanned will degrade the cavity fringe contrast. The extent of coupling between the injection laser and cavity modes and the subsequent effect on the decay intensity depends explicitly on the number of dynamic mode matches that occur during the ringdown or observation time. In the CAPS and cw ringdown techniques previously discussed, sensitivity and wavelength tuning were severely hampered by random dynamic mode matching between the cw injection laser and the cavity. The pulsed CRLAS method of O'Keefe and Deacon was systematically developed to overcome the above interference effects by choosing an input laser whose coherence length was shorter than the cavity mirror spacing.

As seen from the above considerations, mode excitation in the cavity in CRLAS depends explicitly on both the input light and the cavity properties. In a few cases the resultant interference will be easy to predict, while in most it will be complicated by the complex profile of the input pulse convoluted with the cavity mode structure and stability. In such cases, the mode matching between the laser and

ringdown cavity can be essentially random, and no interference phenomena are observable. Up to this point we have only considered the behavior of an empty cavity, focusing on the transmission anomalies associated with frequency filtering of the input light. A more interesting and complex discussion arises when we consider the coherence effects that can arise when an absorber is placed in the cavity.

A simple starting point for the discussion of coherence effects in the ringdown cavity is to again consider the picture presented in Figure 1, wherein the laser input pulse is shorter than the cavity round trip length, and to consider what an absorber inside the cavity sees as the pulse propagates back and forth. If the lifetime of the upper state is much longer than the round trip time of the cavity, the absorber essentially sees a series of pulses that are described by their duration and periodicity. In this case we can obtain the effective frequency spectrum in the molecule frame via a Fourier analysis similar to that presented earlier. The result in this case (long dephasing time) is an enhancement for the absorption probability for transitions that are resonant with the cavity modes and a suppression for off-resonance transitions. This type of interaction has been considered in detail long before the advent of CRLAS, and is the basis for phenomena such as those associated with Ramsey fringes.[41] In fact, the specific case of a long-lived absorber placed in an optical resonator was experimentally explored by Hänsch and coworkers[42] in the late 1970's. This type of coherent interaction is itself independent of the bandwidth of the excitation light in the case where the bandwidth is greater than the transition linewidth. However, the ability to observe this coherent interaction in CRLAS is in fact explicitly dependent on the injection laser bandwidth, as will be discussed later. For cases wherein the input laser pulse overlaps in the cavity, the possibility of the transmission anomalies mentioned above together with the multiple pulse coherent interaction arises if there is a significant periodic modulation of the intracavity light intensity.

The regimes wherein this type of coherent phenomena can occur in CRLAS have been qualitatively discussed by Zalicki and Zare[30] while the net effect on the extracted absorption intensities to date has not been quantified and is still a topic of debate. In this section, some practical considerations are outlined for understanding when a given experimental arrangement carries with it the potential for such effects. It is again relevant to stress that distorted or missing spectral features have not been demonstrated in CRLAS experiments to date and, furthermore, that the potential for them requires that several stringent experimental conditions be met. As is the case in the above discussion of transmission modulation, simple design of the cavity dimensions and tailoring of the input light (e.g., to effect mode matching) is generally sufficient to eliminate any potential for significant distortion of the absorption intensities obtained with CRLAS.

Again consider the case where the upper state lifetime of the molecule is longer than the round trip transit time of the cavity and the injection laser pulse length is shorter than the cavity round trip length. In this case, the effective spectrum "seen" by the molecule is obtained by taking the Fourier transform of the number of pulses that interact with the molecule during its lifetime superimposed on the bandwidth of the input laser. The same condition applies to the observation of two-photon optical Ramsey fringes such as those observed by Solour[43] and Bergquist et al.[44] Those molecules that do not relax to the lower state or appreciably move during the time between successive pulses essentially see the cavity mode spectrum, that results purely from the periodic nature of the interaction. This effect has also been described as the "appearance of modes" by Zalicki and Zare[30] and may be undetectable in CRLAS depending on the line width or lifetime of the upper state in comparison to the injection laser bandwidth (or coherence length). The effective spectrum that results in the molecular frame of reference is similar to that of the effective output of a mode-locked laser. The width of the modes in the molecular frame narrows as the number of pulses increases (i.e., longer lifetime) in a similar way to the mathematical treatments presented earlier to describe energy buildup in the cavity. However, in this case, we do not need to specify the frequency spectrum of the input light, since it is the molecule that imposes the coherence on the system. In the work of Hänsch and coworkers,[42] a confocal geometry was employed to maximize the resultant Ramsey-type modulation of the Doppler-limited background signal by effectively assuring that only a single period was associated with the interaction. A nonconfocal geometry would have resulted in different round trip times, which would have effectively washed out the observed spectral modulation. In addition to the effective filtering of the spectrum imposed by molecule, the transition probability is similarly increased for transition frequencies resonant with the cavity modes. In these limits, wherein the lifetime is longer than the excitation pulse time, there is an additional pulse-propagating effect that has been described by Crisp[45] that causes further deviation from Beer's law behavior of the absorbing medium, which may need to be explicitly included to predict the net result to the absorption intensity.

The difference between the above-cited experiments and CRLAS, however, is that in the former the measured quantity was either molecular fluorescence, light detection due to polarization rotation, or energy imparted to a molecular beam. In these cases, a change in signal is obtained only as a result of the photon-induced change to the molecular system, which results regardless of the bandwidth of the exciting light. In CRLAS, the observable is the fractional change per pass to the total intracavity light intensity. In this case, the laser bandwidth must therefore be explicitly be accounted for, since in some cases only a fraction of the intracavity light will be attenuated. For example, if in the molecule frame a large number of cavity modes are excited yet only a single mode effectively overlaps with the absorption, the fractional absorption of the intracavity field is reduced. In this case, as the ratio of the number of modes excited to the number of modes that overlap with the transition increases, the coher-

ent interaction could go entirely unnoticed. This difference raises questions about the extension of the conclusions drawn in the previous experiments to the observable effects in CRLAS. Accurately predicting the effect on the absorption intensities obtained with CRLAS is clearly complicated by the necessity to explicitly compare the specific transition with the properties of the input laser (such as the coherence length) and the theoretical cavity mode structure and stability, but it is instructive to study limits wherein the effect is either expectedly very small or significant.

In one limit, the injection laser pulse is temporally shorter than the upper state lifetime of the absorber but is much longer than the round trip time of the cavity, which is also to say that the line width of the transition is narrower than the cavity longitudinal mode spacing. Here, the molecule effectively sees a cavity mode spectrum that is comprised of a large number of modes. The attenuation of the intracavity field depends on whether the molecule absorption falls in between, on, or on the shoulder of a cavity resonance, with maximum attenuation occurring when the two coincide. In this case, the per pass attenuation of the intracavity field will be minimal, with the possibility of no detectable absorption occurring (i.e., no detectable change to the decay time). Another limit is realized if the lifetime of the molecule is on the order of a few cavity round trip times and the probe laser bandwidth is not much greater than the absorption line width. In this case, the effective cavity modes seen by the molecule are much broader than in the previous case, and subsequently, the fractional absorption of the laser field per pass will be much greater. The molecule will essentially undergo many excitation−relaxation cycles during the course of the cavity decay time. In this limit, there is potential for a significant effect on the absorption spectrum, with the net result again being an undercalculation of the absorption intensity. Both of the above scenarios require the existence of a discrete cavity mode spectrum, which is possible only for either stabilized confocal resonators or stabilized nonconfocal cavities that are very carefully mode matched. Slight misalignment of the cavity in either case can effectively wash out the cavity mode structure. In some cases, the refractive index change associated with molecular absorption can significantly change or shift the mode spacing of the cavity and must also be accounted for.

Although interference effects in CRLAS can be significant in some experimental arrangements and may in fact lead to interesting new applications, it is again important to stress that they are generally easily avoided and do not prevent effective use of CRLAS as described here. For example, simply avoiding the use of confocal or planar cavities will minimize any problems that could be interpreted in terms of gaps in the cavity mode spectrum. This effectively eliminates both types of interference phenomena discussed above. In the case where the cavity is coherently excited to a significant degree, as long as the laser bandwidth is less than the absorption line width, accurate absorption intensities are generally obtained as long as a decay is measurable, i.e., does not fall below the noise level of the apparatus when in a transmission minimum. We have experimentally found that when transform-limited pulsed laser light is mode matched into short (with respect to the laser pulse length) cavities, the resultant transmission contrast can be significant. However, even in cases where the contrast ratio (transmission maximum to minimum) was higher than 20:1, no significant distortion of the absorption intensities was observed, even when the absorption fell in the minimum of the cavity mode structure. Although the coherence phenomenon described above may lead to interesting new observables, it is again important to note that the potential for distorted or missing spectral features in CRLAS is only of concern in extremely limited cases that are typically not encountered in most experiments.

Laser Transverse Mode Considerations

It is worth elaborating on the role of transverse mode effects in ringdown spectroscopy, since the transverse mode competition in the resonator can lead to interesting nonexponential anomalies in the cavity decay. These phenomena are discussed in detail by Siegman[32] and were first discussed for the specific case of ringdown by Scherer et al.[33] and have been studied in detail in recent papers by Martin et al.[34] and Hodges et al.[46] Higher order transverse modes possess different periodicities due to their different optical paths inside the cavity. For multiple modes, there exists a unique periodicity that can lead to a modulation of the decay, which is commonly referred to as "transverse mode beating". This is diagrammed in Figure 5, which represents a typical decay waveform during cavity alignment. This modulation is generally fast with respect to the decay time, and fitting algorithms will typically average out the effect. We have found that modulation up to ca. 15% of the decay intensity for highly reflective cavities produces very little effect on the fitted decay times. However, as decay times become shorter (e.g., lower mirror reflectivities or high absorption) this modulation can lead to significant fitting problems. To prevent multiple transverse mode excitation, the laser can be mode matched with a telescope to the fundamental mode of the ringdown cavity, i.e., the laser spot size can be coupled to the TEM 00 beam waist of the cavity. For a two-mirror stable resonator configuration where both mirrors have the same radius of curvature (r) and are separated by a distance (d), the beam waist radius of the cavity (D) can be calculated from the expression[36]

$$D^2 = (\lambda/2\pi)(d(2r - d))^{1/2} \qquad (23)$$

where λ is the wavelength. The beam waist defines the planar constant phase surface in the center of the cavity and is the smallest in confocal cavities. The waist can be tailored to the particular application. For example, the beam waist radius our molecular beam apparatus is approximately 1 mm at 500 nm, for mirrors 0.5 m apart with 6 m radii of curvature. An alternative method of mode selectivity is to design the cavity such that diffraction losses are high for the unwanted modes. This can be achieved by

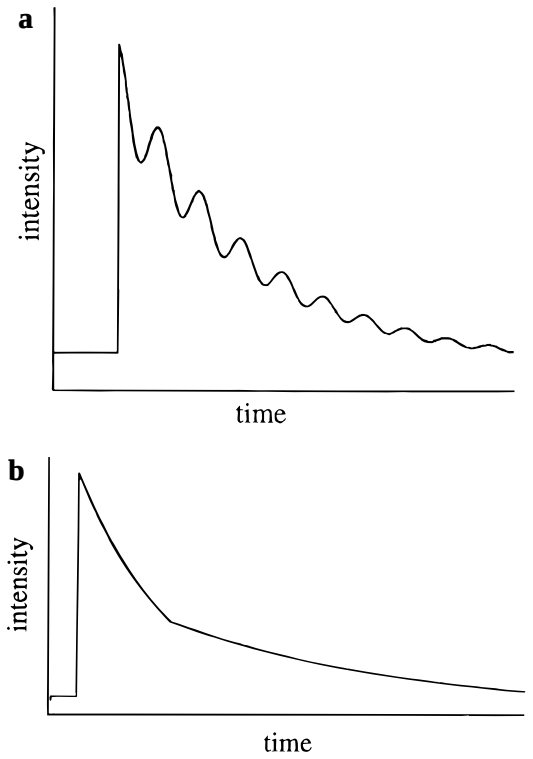

Figure 5. Typical decay modulation exhibited during cavity alignment. In a, poor cavity alignment or high transverse modes of the input laser lead to variations at the detector, as the light samples different regions of the cavity and of the detector. Similar modulation can also result from transverse mode competition in the case of coherent excitation. In b, the multiexponential character of the cavity decay is shown, although exaggerated for the sake of example.

placing limiting apertures inside the cavity or by tailoring the size of the input pulse to the mirror diameter. These types of mode filtering schemes are commonly employed in the design of lasers.[47]

Another type of transverse mode effect that is commonly observed during alignment is that of the beam walking across the face of the detector element as the pulse multipasses the cavity. This effect is due to the variation of the quantum efficiency over the detector surface and is easily differentiated from the mode beating described above by placing a folding mirror before the detector and varying the placement of the light exiting the cavity upon the detector element. In some cases, the beam can actually walk off of the detector element, that can lead to large modulation of the decay. Both of these effects can generally be eliminated altogether by focusing the exit light onto a small region of the detector element with a lens.

Laser modes other than TEM 00 possess both larger cross-sectional areas and nodes and will therefore walk across a larger region of the mirror surface during the ringdown event and are more likely to excite higher order transverse modes of the cavity. Higher order transverse modes can be altogether eliminated by passing the laser light through one or more spatial filters, such as a two-lens telescope with a precision pinhole. In this manner, the transverse profile of the light can be brought to nearly pure TEM 00, which facilitates efficient coupling into the cavity fundamental mode, if so desired.

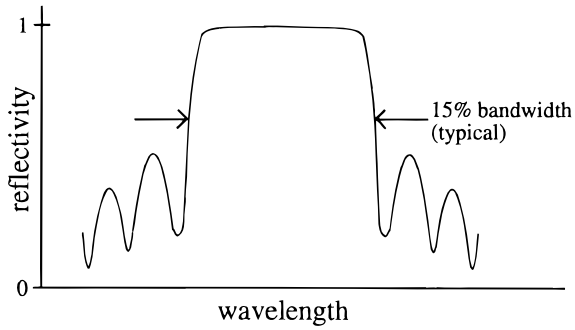

Figure 6. Mirror reflectivity as a function of wavelength. The multilayer dielectric mirrors are only useful within ca. 15% of the design (maximum reflectivity) wavelength. At the wings of the curve, oscillations in the *R* value are evident.

Cavity Mirrors

One final consideration in the discussion of CRLAS sensitivity is the contribution of the cavity mirrors themselves to achievable sensitivity limit. The mirrors employed in the cavity ringdown technique are composed of highly polished substrates with multiple layer dielectric coatings. As many as 40 layers (e.g., metal oxide coatings for visible/UV mirrors) are applied to the substrate. The high reflectivity of these optics is achieved through constructive interference of the multiple reflections from the many ($\lambda/4$) layers of the coating. Figure 6 shows a typical reflectivity curve for the case of layers of alternating high and low indices of refraction.[48] At the wings of the reflectivity curve, oscillations in the *R* value are evident. These oscillations will also be present in the smooth part of the curve, although to a much lesser extent. As higher levels of sensitivity are desired in the CRLAS technique, these oscillations will require background subtraction. Even with the implementation of background subtraction, however, a point will be reached where the uncertainty associated with the mirror reflectivity sets an upper limit on the attainable sensitivity. As the only method currently available to determine the reflectivity of such high quality mirrors is the ringdown method itself, this poses the added difficulty of separating the error associated with mirror phenomena from errors associated with the other factors described above.

From this discussion, it is evident that both high-sensitivity and high-resolution applications of the CRLAS technique can be implemented, if the above constraints are carefully considered. If good TEM laser mode quality is achieved and the light is properly coupled into the resonator, one need only tailor the cavity dimensions to the input light properties. Additionally, the time scale of the event to be probed must be considered, as in the application to transient species or pulsed molecular beams discussed below.

IV. CRLAS of Pulsed Supersonic Jets

In this section, CRLAS data of species generated in laser vaporized molecular beams are presented,

with specific examples chosen to demonstrate the advantages and generality of the technique. In addition, subtleties related to this application are discussed, which are likely to be encountered in other applications involving high-density, transient environments. In our initial application of CRLAS for molecular beam spectroscopy, optical spectra of a variety species were obtained, including C_2, NbO, AlO, Cu_2, and Cu_3.[6] The results of the copper trimer system constituted the first direct absorption gas-phase data obtained for a polyatomic transition metal cluster. Since our work in 1990, we have measured additional bands in the $^2A-^2E$ system of Cu_3 and have obtained rotationally resolved spectra of many other species, including C_3, AlAr, Cu_2, Si_2,[49] Nb_2, Al_2,[50] CuSi,[51] AgSi,[52] AuSi,[53] PtSi,[54] and AlC. Some of these results will be presented later.

In these molecular beam studies, a supersonic beam of clusters is formed by vaporizing a sample rod in a stainless steel housing while a pulsed valve backed with 10−20 atm of buffer gas is fired. The mixture is then expanded through a nozzle into a Roots pumped vacuum chamber, forming a free-jet expansion of internally cold molecules. Simultaneously, the pulsed molecular beam is intersected by the ringdown laser pulse at the cavity waist of the resonator. The transient molecular beam is timed to coincide with the ringdown event, which is typically tens of microseconds. The ringdown is monitored with a photomultiplier, amplified, digitized, and transferred to a PC for analysis. The total cavity losses are deconvoluted from the measured cavity decay time using eq 11. Molecular absorption intensities are then obtained by subtracting the base-line losses of the cavity, which are determined while the laser is off-resonance with all molecular transitions. Typically, several laser shots are averaged per wavelength increment, primarily to reduce the noise caused by molecular beam fluctuations.

Before these initial experiments, it was not clear whether the transient nature of the molecular beam would pose a serious problem in extracting accurate relative absorption intensities. This problem would primarily arise from variations in the molecular internal temperature and concentration over the time scale of the ringdown event. For example, a molecular beam traveling at 2 km/s would travel through the 2 mm width of the probe laser spot in 1 μs, which is equivalent to roughly 300 round trip times for a 0.5 m cavity. This means that for a typical 10 μs ringdown time, the total decay has sampled a region which is ca. 10 times the length of the laser beam width. If the species concentration or temperature is not constant, or if significant saturation of the transition occurs during the ringdown, the resultant relative absorption intensities will not necessarily be accurate. The effects associated with varying species state density were explored by bracketing the fitted region of the decay and changing the delay time of the ringdown laser with respect to the vaporization laser and observing changes in the associated absorption intensities. In doing so, the region with maximum absorption was identified, and the changes to the relative absorption intensities were minimized. The ability to extract accurate relative absorption intensities in the case of transient molecular beams will be exemplified later in presentation of the spectra of transition metal silicides, which are directly compared with Franck−Condon simulations.

The extent to which cavity alignment would be affected by refraction and scattering in the beam region was also unknown, due to the sensitive multipass nature of the technique. In the specific case of laser-generated plasmas, shot to shot fluctuations in the molecular beam composition can be severe, with the potential for large scattering contributions and lensing effects. In the case of cavity losses due to nonresonant processes, noise contributions are more severe since they scale with the square of the number density, whereas molecular absorption will vary approximately linearly with concentration. This fact required that the most stable part of the supersonic expansion be identified. The above effects required that both extremely stable sources be employed and that careful timing of the two events be maintained. Although these effects could be minimized, they limited the achievable sensitivity to typically 2−10 ppm for most metal cluster studies and 10−50 ppm in the case of carbon cluster beams. Several of the above subtleties are demonstrated in the spectra presented later.

Applications to Metal Cluster Systems

One of the primary goals of cluster research has been to deduce detailed molecular descriptions for bulk phenomena. In the case of transition metals, there are several areas of current interest. The first topic of interest is that of incipient metallic bonding in metals and metal alloys, in terms of the specific contributions to bonding from the associated atomic orbitals.[55] A second area of interest is that of size-dependent effects, wherein variations in the physical properties due to packing, delocalized orbitals, etc., lead to collective phenomena, such as plasmon resonances.[56] Understanding the evolution of the metallic state as a function of cluster size is another topic of importance to the development of microelectronics devices.[57] The mechanisms responsible for the catalytic behavior of certain metals are also of current interest. In addition to understanding bulk phenomena, small clusters may be important in the context of understanding the properties of the different stoichiometric phases that can occur at interfaces between dissimilar materials.

Gas-phase metal cluster research offers a unique route to understanding a wide variety of the above active areas of research, since information on the ground and excited states of specific systems allows us to extract quantities such as binding energies, bond lengths, molecular orbital occupancies, and ionization potentials. The ability to readily produce metal clusters in laser vaporization molecular beam sources[57,58] has greatly facilitated these efforts. The detailed data obtained in these studies, together with the increased sophistication of the theories used to model metal cluster systems, serves to enhance our understanding of the fundamental properties of metal or metal-containing species.

In this section, CRLAS electronic spectra of several bare metal and metal silicide clusters will be pre-

sented. The systems chosen for presentation in this section were selected in part as proof of the generality of the CRLAS method. For the copper dimer, emphasis is placed on the comparison to data obtained with the complimentary techniques of R2PI and LIF. Following this, the first gas-phase data of the $2^3\Pi_g$ predissociative state of Al_2 will be presented,[50] as an example of the applicability of the CRLAS method to states that are altogether invisible to both R2PI and LIF. Data for the copper trimer[6] are then presented and directly compared with the data obtained in R2PI studies. Again, the results of the copper trimer studies underscore the advantages of employing a direct absorption method for the study of metal cluster species that undergo predissociation in the excited state. Finally, data will be presented for the coinage metal silicide diatoms,[51−53] which include the first gas-phase spectroscopic data for both copper and silver silicide. This application of CRLAS for an entirely new class of molecular clusters serves as an example of the power of the ringdown method for applications in the field of cluster science.

Copper Dimer

The copper dimer is perhaps the most thoroughly studied of all transition metal diatoms. A wealth of experimental data have been obtained in the last decade, allowing a direct test of theoretical models of ground- and excited-state bonding. In the first-order description, d-orbital contributions to bonding in dicopper are ignored, and the two ground-state atoms ($^2S_{1/2}$) combine to form the $4s\sigma^2$ bond of the $^1\Sigma_g$ ground state. Although this simple picture accounts for the correct ground-state configuration, it does not account for all of the experimentally determined properties, such as the binding energy. The first two excited states in dicopper are due to a 3d−4s promotion in one of the atoms, at the asymptotic limit. These states (the A and B states) were both assigned as being of Σ symmetry in previous studies. In two independent studies, LIF[59] and R2PI[60] spectra of a new C state were also obtained, though neither achieved the rotational resolution necessary for a positive spectral assignment. In our initial CRLAS studies, data on the C state were also obtained, but, again rotational features were not resolved.[6] Later studies performed with a higher resolution (0.04 cm^{-1}) dye laser facilitated rotational resolution of the C−X and B−X bands, which are shown in Figures 7 and 8. Of particular interest in the C−X band is the obvious Q-branch, indicating that the C state is of Π symmetry. The relative intensity of the C−X band compared to that of the B−X system suggests that the C state is also a singlet state (i.e., $\Delta S = 0$).

Just prior to our CRLAS measurements, Page and Gudemann[61] had also obtained rotationally resolved spectra of the C−X band, using the technique of laser-induced fluorescence (LIF). Comparison of our CRLAS data to their LIF data reveals important differences that are due to the different techniques and sources employed. The colder internal temperatures of our laser vaporization source, compared to those of the sputtering sources used in the LIF work, produced rotationally resolved spectra that were significantly less congested. Of greater importance,

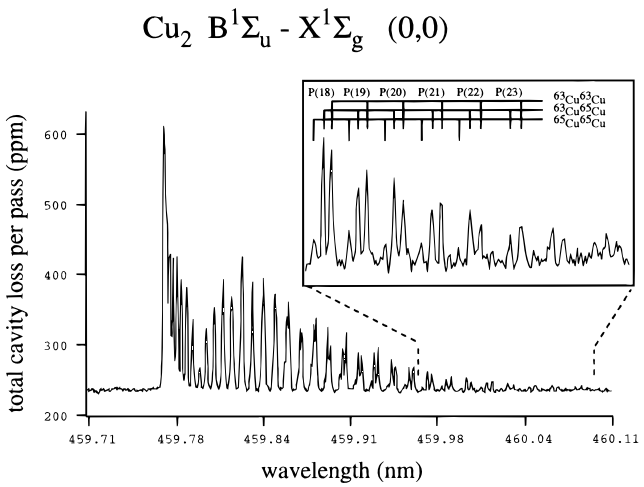

Figure 7. CRLAS spectra of the B−X (0−0) rovibronic band of copper dimer. The inset shows the detail of the P-branch, wherein the rotational isotope effect is evident. In this scan, the total cavity losses per pass are plotted, which include the mirror and scattering losses. The respective absorption intensities are obtained by subtracting the nearly constant baseline.

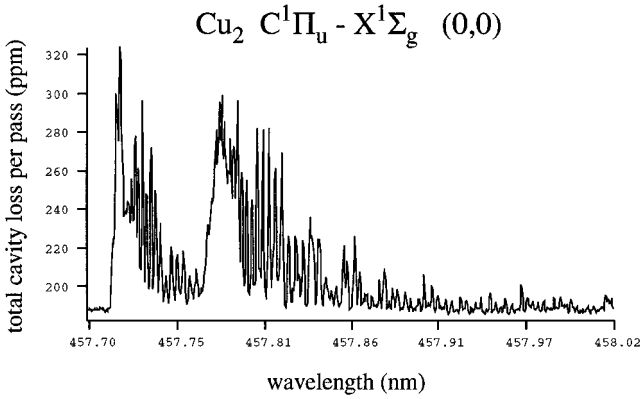

Figure 8. CRLAS spectra of the C−X system of Cu_2, obtained with a probe laser resolution of 0.04 cm^{-1}. The obvious Q-branch indicates that the upper state is of Π symmetry. The intensity of this band is ca. 1/2 of that of the B−X system, in contrast to the intensities obtained in fluorescence and resonance ionization studies. Again, the total cavity losses (per pass) are plotted.

however, is the difference in the relative intensities of the B−X and C−X band systems among the CRLAS data, the LIF spectra obtained by Page and Gudemann,[61] and the R2PI results of Powers et al.[60] In both of these LIF and R2PI studies, the C−X band was measured with nearly twice the intensity of the B−X system, in contrast to our direct absorption data, where the C−X system band intensity is only ca. 50% that of the B−X system. This difference in relative intensities suggests that excited state dynamics are distorting the band intensities in both the R2PI and LIF data, since our absorption data should only suffer from the line-broadening effects associated with short upper state lifetimes. The ability of CRLAS to obtain quantitative intensity information is further demonstrated in the rotational isotope splittings observed in high J P-branch lines of the B−X system, as shown in the inset of Figure 7. The intensities of the rotational lines reflect the relative abundance of the three diatom isotopomers ($^{63}Cu_2$, 47%; $^{63}Cu^{65}Cu$, 43%; $^{65}Cu_2$, 10%) convoluted with the associated 5:3 intensity alternation derived from spin

statistics. These features have not been resolved in previous studies. The copper dimer data demonstrates the ability of CRLAS to obtain quantitative absorption intensities with signal to noise levels comparable to the previous LIF and R2PI experiments.

Aluminum Dimer

In this section, data for the $2^3\Pi-{}^3\Pi X$ band system of the aluminum dimer[50] are presented that demonstrate the ability of CRLAS to access states that are altogether invisible to LIF and R2PI. Although rigorous scans for this system were performed independently in both R2PI[62] and LIF[63] experiments in this same spectral region, no data were obtained. As suggested in the R2PI and LIF work, and as predicted in the theoretical work of Bauschlicher,[64] the CRLAS data suggest that the $2^3\Pi$ upper electronic state undergoes rapid predissociation, explaining the elusive nature of this band system to "action" spectroscopies.

A review of previous experimental data for Al_2 has been presented recently by Fu et al.,[62] and we will therefore primarily focus on information relevant to the $2^3\Pi g-X^3\Pi u$ band system. Of particular interest in this body of work are the differences in the data obtained by the various techniques employed. For example, the $A^3\Sigma_g^-$ state has not been observed in the molecular beam studies, presumably due to strong cooling in the expansion and/or unfavorable selection rules. Similarly, the 1 and $2^3\Pi_g$ states had been observed only in matrix isolation direct absorption studies. The first of these two states ($1^3\Pi_g$) is predicted to be purely repulsive.[64] In contrast, the $2^3\Pi_g$ state is predicted to be bound by several eV[64] and has been assigned to a band system observed in an early matrix study,[65] with an origin around 410 nm and a measured upper state vibrational frequency of ca. 238 cm^{-1}. This same band system was later searched for in two independent LIF[63] and R2PI[62] studies, but was not observed. With these points in mind, a search was made for this band system with the CRLAS apparatus.

Initially, three distinct features between 413 nm and 405 nm were measured (shown in Figure 9), which we assigned to a single vibronic progression with an associated vibrational frequency of 210 cm^{-1}($\pm$4 cm^{-1}) and anharmonicity of ca. 8 cm^{-1} ($\pm$2 cm^{-1}). Relative intensities for the three bands were consistently measured to be 4:2:1 for the 0−0:1−0:2−0 band systems, respectively. Following these low-resolution scans, high-resolution scans ($\delta\nu \approx 0.04$ cm^{-1}) were performed yet no rotationally resolved features were observed. This lack of rotational structure is consistent with a transition to a predissociative upper state, with an associated lifetime of less than ca. 10 ps.

To assist in assignment of this band system, source conditions were altered in an attempt to populate excited vibrational or spin-orbit levels of the lower electronic manifold. The results of these scans are partially shown in Figure 10. Under these "hot" source conditions, two sharply blue-degraded bands (labeled A and B) were observed ca. 41 and 79 cm^{-1} to the red of the 0−0 band, respectively. Similarly,

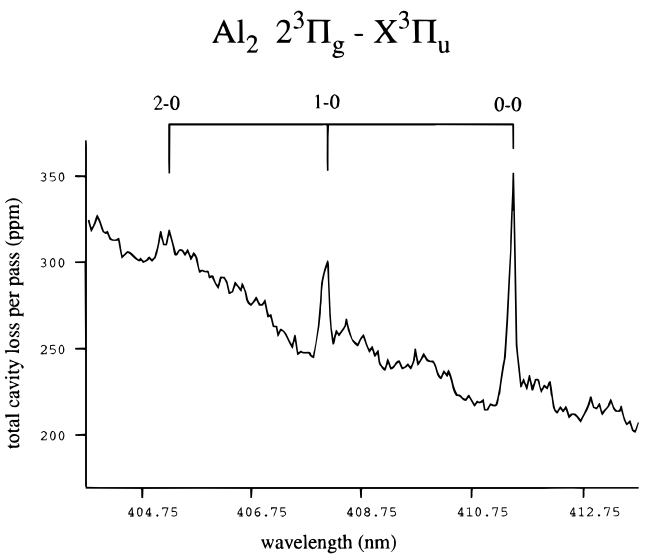

Figure 9. Low-resolution CRLAS spectra of the $2^3\Pi_g-X^3\Pi_u$ system of Al_2, obtained under *cold* clustering conditions, with a laser bandwidth of ~0.3 cm^{-1}. The absence of bands to the red of the 411 nm band indicates that it is the vibronic origin. Because the total cavity losses are plotted, the reflectivity curve of the mirrors leads to a sloping base line.

additional bands were also observed to the red of the 1−0 band under these same conditions, with, again, the same spacing. These additional bands could not be explained as vibrational hotbands, on the basis of the previously determined ground-state vibrational frequency and the 210 cm^{-1} upper state frequency observed. On the other hand, the additional bands were consistent with transitions out of excited spin-orbit states of the lower electronic state. In this case, given that the two excited $^3\Pi_1$ and $^3\Pi_2$ spin-orbit states of the ground state Al_2 are known to be at 30.4 and 63.4 cm^{-1} above the ground $^3\Pi_0$ state,[62] an assignment for the additional features as $^3\Pi_0-{}^3\Pi_0$, $^3\Pi_1-{}^3\Pi_1$, and $^3\Pi_2-{}^3\Pi_2$ sub-bands of the $^3\Pi-{}^3\Pi$ manifold would require an *inverted* upper state with an associated spin-orbit splitting constant of ca. 8 cm^{-1}, as shown in the energy level diagram of Figure 11. In this case, the assignment for the additional bands (features A−D for both the 0−0 and 1−0 bands) is as shown in Table 3. High-resolution scans of these additional bands similarly yielded no additional rotational structure, consistent with the hypothesis of rapid upper state predissociation.

Although we cannot precisely determine the upper state lifetime from the CRLAS data, we can set a lower limit for it by careful inspection of the R-branch head of the 0−0 band. If we assume the FWHM of the shoulder of the bandhead places a lower limit on the line width of all of the rotational transitions, we arrive at a lifetime of >2 ps. This lifetime would effectively wash out individual rotational features. These data on the aluminum dimer demonstrate the ability of CRLAS to access states that may be invisible to techniques such as LIF and R2PI, which rely on favorable upper state dynamics.

Copper Trimer

The copper trimer is the most widely studied transition metal trimer, both theoretically and ex-

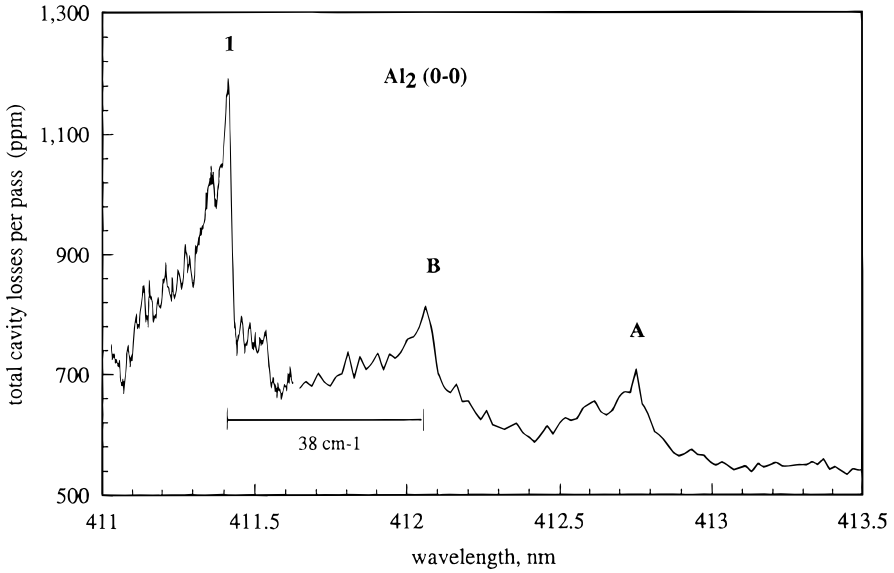

Figure 10. CRLAS spectra of the aluminum dimer taken under *hot* source conditions. The appearance of only two additional bands to the red of band 1 (the 0−0 band) is consistent with the population of excited spin-orbit levels of the ground state.

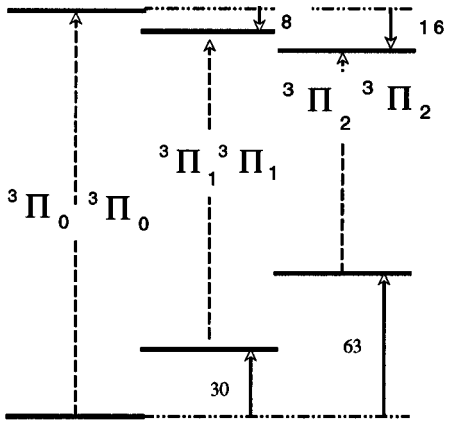

Figure 11. Energy level diagram of the $2^3\Pi_g-X^3\Pi_u$ system of Al_2, showing the spin-orbit levels of the ground and excited states. The energy defects of the associated spin-orbit levels are given in cm^{-1}.

Table 3. Vibronic Assignments for the $2^3\Pi_g-X^3\Pi_u$ System of Al_2, Including the Observed Transitions out of the Excited Spin-Orbit States of the Ground Electronic Manifold

band no.	frequency, cm^{-1}	assignment
1	24 306	0−0
2	24 502	1−0
3	24 681	2−0
A	24 227	$^3\Pi_2-^3\Pi_2$ (0−0)
B	24 268	$^3\Pi_1-^3\Pi_1$ (0−0)
D	24 463	$^3\Pi_1-^3\Pi_1$ (1−0)

perimentally. Early experiments include the matrix isolation work of Moskovits and Hulse[66] and the jet-cooled R2PI experiments of Morse et al.[67] In the Morse et al. R2PI and photodepletion experiments, 12 vibronic bands were measured in the 525−545 nm region and assigned to transitions from the $^2E'$ ground vibronic state to an excited state of $^2E''$ symmetry. Later LIF experiments conducted by Rohlfing and Valentini[68] provided evidence for a reassignment of the upper state to $^2A'$ symmetry, due to the fact that additional bands were observed when pumping a vibronically excited level of the upper state. In our initial CRLAS Cu_3 experiments, data for the above (540 nm) band system were obtained[6] and indicated reassignment of one of the features first seen by Morse et al. Additionally, new bands were measured that were assigned to transitions originating out of the higher energy Jahn−Teller component of the fluxional ground state.

In the case of a strong Jahn−Teller interaction in the ground state of Cu_3, the $^2E'$ state, which is a maximum on the potential surface, is split into lower energy $^2A_1$ (acute) and $^2B_2$ (obtuse) states with C_{2v} symmetry. According to Bauschlicher et al.,[69] these two minima are predicted to be nearly degenerate. For an e′ vibration of a $^2E'$ electronic state, the addition of one quanta in the degenerate bend leads to states of $^2E'$, $^2A_1'$, and $^2A_2'$ symmetry. For the case of D_{3h} symmetry, these levels are degenerate. In the presence of a strong Jahn−Teller effect, this degeneracy is lifted, leading to two degenerate A states and a higher energy E state. In the work of Morse et al.,[67] the A state was measured to be roughly 15 cm^{-1} above the $^2E'$ ground state. In the limit of strong Jahn−Teller stabilization, this energy difference would represent the tunneling splitting between the three equivalent C_{2v} minima. This assignment is supported by our CRLAS data, which includes two new previously unobserved transitions originating from the $^2A'$ state.

Comparison of the CRLAS spectra shown in Figure 12 with the R2PI and depletion data of Morse et al. again reveals the advantages associated with a direct absorption probe for studying predissociative states. We have used the same numbering convention as that of ref 67 for the sake of clarity. As a result of upper state predissociation, the intensities of bands 5 and 7 in the R2PI work are substantially lower than that of band 2. In contrast, the CRLAS data exhibit similar intensities among these three bands, with peak 5 being the strongest. The relative intensities evident in the absorption data more likely reflect the associated relative transition probabilities for this system, since they are not affected by predissociation. Another discrepancy between the CR-

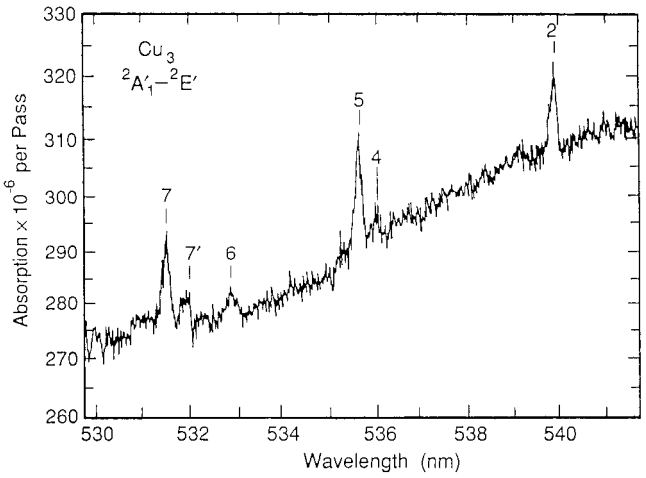

Figure 12. CRLAS spectrum of the copper trimer obtained with a laser resolution of 1 cm^{-1}. The CRLAS band intensities are very different from those obtained in R2PI and LIF studies, presumably due to upper state predissociation. The sloping base line reflects the variation in mirror reflectivity.

LAS data and that of the previous work concerns the assignment of band 4, which had been previously invoked to excitation from the singly excited v_1 level of the ground state to the triply excited degenerate bending mode of the upper state.[67] If this additional band in fact originated from the vibrationally excited ground state, a second band at 538.4 nm would be expected, with reasonable intensity. The absence of a band at this wavelength, presumably due to a lack of population in the ground state, argues against this assignment. An alternative assignment for this band is that it is due to a transition from the Jahn−Teller active $^2A'$ state located 15 cm^{-1} above the ground state, which is precisely the defect observed between bands 4 and 5. A second point of interest involves the band labeled 7′ in our spectra. This band does not appear at all in the R2PI work of ref 67. The energy difference between bands 7 and 7′ is also ca. 15 cm^{-1}, the same as the energy difference between bands 4 and 5. Since the vibronic species of band 7 are A'_1 and E′, excitations from the Jahn−Teller active $^2A'$ state to the $2\nu_1{}^2A'_1$ are fully allowed. We therefore assigned this additional band as originating from the slightly higher energy Jahn−Teller component of the lower state. Since our initial Cu_3 results, two additional bands have been observed that also exhibit the expected 15 cm^{-1} splitting and have been assigned as $3\nu_1{}^2A_1' - {}^2E'$ and $3\nu_1{}^2A1' - {}^2A'$. Table 4 lists the absorption bands measured to date with CRLAS, with the corresponding assignments. Figure 13 demonstrates the improved sensitivity of our more recent Cu_3 data. The rotational structure in this high resolution spectrum is further evidence of the a-type transition in this A−E vibronic system, with the expected red degraded Q- and R-branch heads.

In an effort to obtain additional data on the copper trimer, we have scanned large regions of the visible spectrum (450−650 nm), with no additional features observed. Of particular interest in this note is the lack of bands seen by Knickelbein, who has reported a strong system in the 518 nm region.[70] It is possible that these transitions (seen in photodissociation experiments) do not originate from the ground state of Cu_3, since it is unlikely that we would not have observed them with CRLAS with the current sensitivity. The above data on the copper trimer system demonstrate the freedom from upper state dynamics, which can significantly distort band intensities in "action" spectroscopies such as R2PI, as well as the ability to probe polyatomic molecules with sensitivity comparable to that of LIF and R2PI.

Table 4. Vibronic Bands and Assignments for the Copper Trimer

band no.	wavelength[a] (Å)	Assignment[b]
1	5422.5	$^2A_1-1\omega_1{}^2E'$
2	5398.5	$^2A_1-{}^2E'$ (origin)
4	5360.0	$1\nu_1-A'$[c]
5	5356.0	$1\nu_1-{}^2E'$ (origin)
6	5328.2	$1\nu_2-{}^2E'$ (origin)
7′	5318.5	$2\nu_1-A'$[c]
7	5314.4	$2\nu_1-{}^2E'$ (origin)
8	5290.5	$1\nu_1 1\nu_2-{}^2E'$ (origin)
9	5278.5	$3\nu_1-A'$[c]
10	5275.0	$3\nu_1-{}^2E'$ (origin)

[a] Wavelengths are band centers and are ± 0.5 Å. [b] Upper state designations for bands 2−10 uses the normal mode nomenclature of ref 67. [c] A′ designates the higher energy ground state Jahn−Teller component, which is estimated to be ca. 15 cm^{-1} above the lowest E′ level.

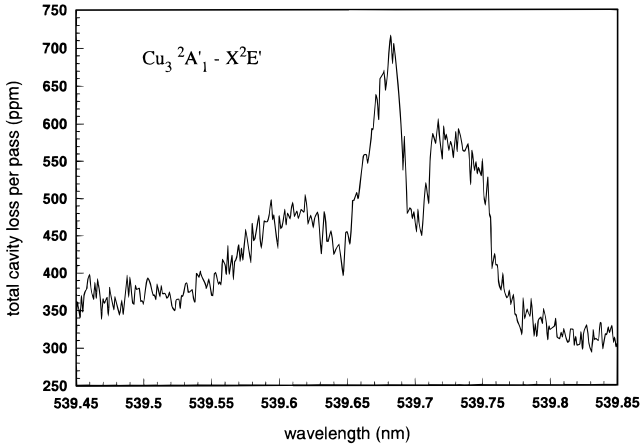

Figure 13. High-resolution scan of the 0−0 band of the $^2A-{}^2E$ system of copper trimer, which exhibits red-degraded Q- and R-branch heads. The improved signal is due primarily to source design modifications.

Metal Silicides

In the last decade there has been much interest in the formation mechanisms and properties of metal silicides in the bulk phase, primarily motivated by the associated consequences of silicide formation at the metal−silicon interface for semiconductor and microelectronics devices. Numerous solid-state experimental techniques have been implemented to detect the presence of metal silicides and measure their respective properties, such as (Schottky) barrier heights and contact resistances.[71] In particular, the coinage metal silicides have received much attention, due to their common use in electronic devices, and their possible use in micro circuitry, such as very large scale integrated (VLSI) circuits. Several solid state studies have focused on the trends observed for silicide formation in Cu, Ag, and Au films that have been deposited on silicon substrates. In spite of the large body of solid state work, the formation mech-

anisms and properties of metal silicides are still not well characterized.

In an effort to characterize the fundamental properties of molecular transition metal silicides, we have employed CRLAS for the study of jet-cooled metal−silicon complexes. Our initial efforts have focused on the coinage metal silicides, Cu_xSi_y, Ag_xSi_y, and Au_xSi_y, since the sodium like valence of these metal atoms provides a simple starting point for understanding transition metal−silicon bonding trends. Spectra for copper, silver, and gold silicides will be presented, followed by a discussion of the similarities and differences observed in the bonding and properties in these three compounds.

Copper Silicide

As copper possesses the simplest electronic configuration of the transition metals ($3d^{10}4s^1$), it serves as a benchmark for understanding the bonding interactions that occur between transition metals and silicon. Several recent thin-film studies have focused on the interaction of Cu deposited on silicon substrates and subsequent copper silicide formation at the copper−silicon interface.[72−75] In these studies, the formation of various phases of copper silicides has been verified, even at deposition temperatures as low as 313 K.[75] In addition to the study of formation mechanisms, electrical properties at the metal−silicon interface have been correlated with the specific Cu_xSi_y stoichiometric phases present.[76] Although solid-state spectroscopic and gas-phase mass spectrometric studies of some copper silicides have been performed, no gas phase spectroscopic data prior to our CRLAS data[51] have been reported. Similarly, there currently exists very little theoretical literature on molecular metal silicide systems. To the best of our knowledge, only three molecular silicides, PdSi, CrSi, and NiSi, have been studied at the ab initio level.[77−79] Even though no ab initio studies have been carried out on CuSi, considerable insight can be inferred from the work on NiSi, owing to the approximate bonding similarities expected between Ni and Cu.

A first-order description of the ground-state bonding in the CuSi diatom involves combining ground-state Cu atoms ($3d^{10}4s^1$) with the $3s^23p^2$ configuration of Si. Considering only the $3d^{10}4s^1$ configuration of the copper atom is justified by the fact that copper has been shown to readily form chemical bonds in this state (e.g., Cu_2, Cu_3, CuNi, CuAg, etc.).[80] In the L−S coupling limit, this amounts to finding the states resulting from combining ^{2}S Cu atom with ^{3}P, ^{1}D, and ^{1}S states of the Si atom. States resulting from the combination of ^{2}S and ^{3}P terms are of $^2\Sigma$, $^2\Pi$, $^4\Sigma$, and $^4\Pi$ symmetry.[81] Similarly, possible states resulting from the ^{2}S and ^{1}D combination possess $^2\Sigma$, $^2\Pi$, and $^2\Delta$ symmetry, while those resulting from the addition of ^{2}S and ^{1}S atomic states produce only a $^2\Sigma$ state. Since the ground state of Si is ^{3}P, first order considerations would predict the ground state of CuSi to be of $^2\Pi$ symmetry, derived from the pairing of the $s\sigma$-electrons and the remaining lone $p\pi$ electron. In the event that bonding arises from excited Si asymptotes, a $^2\Sigma$ state would be most likely. The CRLAS data are consistent with either of these possibilities;

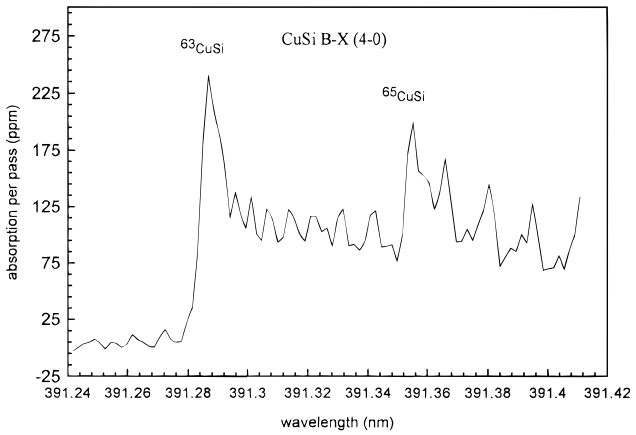

Figure 14. CRLAS spectra of the 4−0 vibronic band of the B−X system of CuSi, obtained with a laser bandwidth of ca. 0.3 cm^{-1}. The two bandheads are due to the two dominant isotopes of the CuSi diatom. This vibronic isotope shift allows determination of the carrier as well as the correct vibronic assignment. The base-line losses of the cavity are subtracted to yield the losses due only to absorption.

however, congestion in the origin region has precluded definitive assignment. Due to the observed lack of Q-branches, it is only possible to rigorously assign these bands as belonging to $\Delta\Lambda(\Omega) = 0$ transitions. For this reason, we adopt the $^2\Sigma$ lower state assignment for the following discussions, with a strong possibility that the observed bands are in fact due to $^2\Pi-^2\Pi$ transitions, wherein the expectedly weak Q-branches are not resolved.

Rovibronic spectra of the B−X system of CuSi were obtained in the UV−vis region extending from 410 to 380 nm and consist of a single vibronic progression in the upper electronic state. The B label for the upper electronic state was adopted on the basis of the fact that the electronic origin is likely too high in energy to correspond to the first excited states of either the copper or silicon atom, taking into account estimated upper and lower state well depths. In the B−X band system, a total of eight vibronic bands were observed, seven of that exhibited well-resolved vibrational isotope shifts. The bandhead frequencies of the lighter isotope ($^{63}Cu^{28}Si$) fit adequately including only first-order anharmonicity, yielding an upper state vibrational frequency of 278 cm^{-1} with an associated anharmonicity of 2.8 cm^{-1}. Attempts made to increase population in the excited vibrational levels of the ground electronic state (decreasing gas pressure, increasing vaporization energy, etc.) produced no additional features, presumably due to efficient vibrational cooling obtained in the expansion. In spite of this, the observed isotope shifts allowed inference of the ground-state frequency, which was found to be ca. 330 cm^{-1}. Rotationally resolved spectra allowed the determination of the rotational constants and associated bond lengths of the ground and upper electronic states. Verification of the vibronic assignment in the upper state as well as the spectral carrier itself was facilitated with an analysis of the measured vibronic isotope shifts.

Typical low-resolution CRLAS spectra of the B−X system of CuSi are presented in Figure 14, where the vibrational isotope shift 4−0 vibronic band is shown.

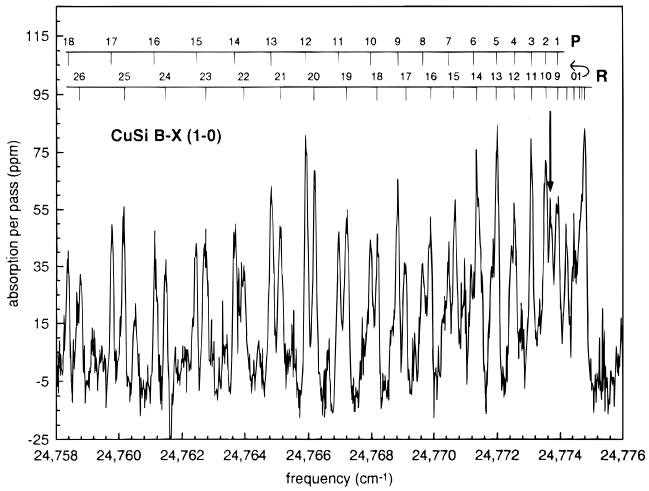

Figure 15. Rotationally resolved spectra of the 2−0 vibronic band of CuSi obtained with a laser bandwidth of ca. 0.04 cm^{-1}. The rapid bandhead formation in the R-branch indicates the significantly reduced bond strength of the excited state.

Table 5. Molecular Constants for the B−X System of CuSi

	X	B
ν_{oo} (B−X)		24 501.6
B_e	B_0 = 0.164 80(21)	0.1295(5)
r_e (Å)	(r_0) 2.298	2.60
α_e	n.a.	0.0021(5)
$D_o \times 10^7$	1.64 (est)	1.12 (est)
ω_e	330 (15)	277.92(4)
$\omega_e\chi_e$	n.a.	2.818
D^e	n.a.	0.849 eV

From the two naturally abundant isotopes of the copper atom (^{63}Cu:^{65}Cu = 69:31) and the single dominant isotope of the silicon atom (^{28}Si:^{29}Si:^{30}Si = 92:5:3), two isotopic CuSi molecules (^{63}Cu^{28}Si and ^{65}Cu^{28}Si) are expected to dominate the observed spectra.

From molecular orbital considerations discussed earlier combined with the fact that the observed spectra exhibited no Q-branches, the bands were fit as $^2\Sigma-^2\Sigma$ transitions, The signature of such a band system will be a splitting of each of the rotational lines into a doublet, the splitting of which will increase linearly with N. In our case, due to the limited bandwidth of our probe laser (0.04 cm^{-1}), this splitting is not expected to become resolved, except for very high N, where a broadening of the lines might become apparent. This leads to a band system that essentially looks the same as a $^1\Sigma-^1\Sigma$ system and would similarly fit equally well as $^2\Pi-^2\Pi$ transitions. Figure 15 shows the rotationally resolved spectra of the 1−0 band, with the rotational assignment as indicated. One feature common to all of the observed bands is the rapid bandhead formation in the R-branch, consistent with the large decrease in vibrational frequency and increase in bond length upon excitation into the upper electronic state. All of the spectroscopic constants for CuSi derived from this work are listed in Table 5. Assuming a Morse potential, an upper state well depth of 0.84 eV is predicted from the table while the lower state cannot be predicted due to a lack of information.

Comparison of the experimentally determined molecular constants of CuSi with those predicted for NiSi in the ab initio study of Shim and Gingerich[78] and Haberlandt[79] provide a consistent picture of the bonding in these two transition metal silicides. In both species, bonding between the metal and silicon atom is primarily of sσ character, as expected for a copper compound. Using the predicted bond length for NiSi from ref 78, a rotational constant for NiSi of 0.18 cm^{-1} would be expected for the ground state, slightly larger than the 0.165 cm^{-1} constant experimentally determined for CuSi. This result is consistent with a more strongly bound nickel species, implying an additional bonding contribution from the open Ni d-orbital. Similarly, comparison of the predicted ground state vibrational frequency of NiSi with the CuSi value inferred above is also consistent with stronger NiSi bonding. Trends in the properties derived above were further explored in studies of the other two coinage metal silicides, AgSi and AuSi.

Silver Silicide

The formation mechanisms and molecular properties of silver silicides have been the focus of a large body of solid state experimental studies in the last two decades. As with copper silicides, the goals of this research include deducing electrical properties of silver−silicon junctions,[82] studying the glass-forming properties of Ag−Si alloys,[83,84] and characterizing Ag−Si surface structures and properties.[85−88] In spite of the large number of bulk phase studies, almost no gas-phase data for silver silicides exist. In fact, the only previous gas-phase work on silver silicides we are aware of is the measurement of the dissociation energy of the AgSi diatom in the mass spectrometric studies of Riekert et al.[89]

To address this deficiency and gain insight into the bonding trends of the coinage metal silicides, spectral scans for silver silicides produced in a supersonic molecular beam were performed throughout the visible and near-UV. A total of 20 rovibronic bands between 365 and 385 nm were observed. Analysis of the bands yielded spectroscopic constants for the X, B, and C states of AgSi. The first-order molecular orbital picture for AgSi is essentially the same as CuSi above. This combined with the apparent lack of Q-branches and spectral congestion at the origin in the observed spectra and again leads to band assignments for both vibronic systems of either $^2\Sigma-^2\Sigma$ or $^2\Pi-^2\Pi$. For the purpose of the following discussion, the $^2\Sigma$ states are adopted, while the B and C upper state designations were adopted on the basis of the likelihood that the observed transitions are too high in energy to correspond to the first excited state. Additionally, unresolved bands that are suspected to be due to AgSi were observed much farther to the red. As with copper silicide, the rotational analyses together with the measured vibronic isotope splittings uniquely determined both the spectral carrier and the vibronic assignment. The data were calibrated using the known UV spectra of the C_3 cluster radical,[90] which is also readily produced in our plasma reactor source by either seeding the helium carrier gas with methane or bubbling it through a variety of organic solvents.

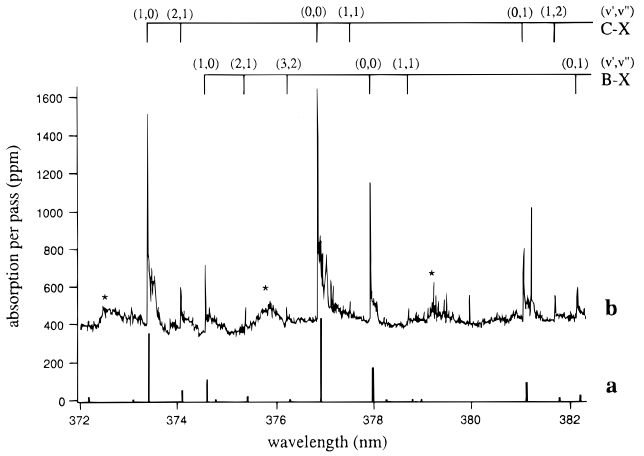

Figure 16. Low-resolution scan of the C,B−X systems of AgSi, with comparison of the measured relative intensities to those predicted in a Frank−Condon simulation, using experimentally determined constants and assuming a vibrational temperature of 300 K. The asterisks denote bands of the H−X system of Si_2, which is readily produced in the plasma reactor.

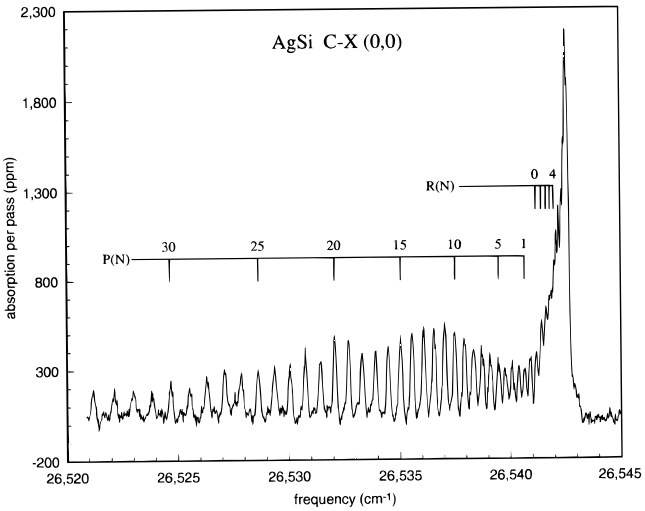

Figure 17. Rotationally resolved CRLAS spectrum of the 0−0 band of the C−X system of AgSi, with the rotational assignment as indicated.

A low resolution scan of the C, B−X systems of AgSi is shown in Figure 16, while the rotationally resolved spectrum of the C−X origin band is shown in Figure 17. Vibrational energy levels (of the $^{107}Ag^{28}Si$ isotope) for the respective states were derived from bandhead positions and were adequately fit including only first-order anharmonicity. Initial attempts to fit the B state as originating out of excited spin-orbit levels of the ground state (in the event of a $^2\Pi$ ground state) proved unsuccessful, making it necessary to invoke a second upper electronic state. A point of interest in the intensities of the observed transitions is the relative intensities of the 0−0, 1−0, 1−1, and 0−1 bands. For transitions out of the ground vibronic level, $\Delta v = 0$ transitions are favored, whereas for transitions out of the excited vibrational levels of the ground state, $\Delta v = 1$ transitions are favored. This effect must be a result of the associated Frank−Condon (FC) factors, since population arguments alone would lead to 1−1 transitions that should be of greater or equal intensity to the 0−1 bands. From the FC analysis presented later, this is indeed found to be the case.

Table 6. Molecular Constants for the $^{107}Ag^{28}Si$ Molecule[a]

	B	*B*	*C*
ν_{oo}		26 462.18(4)	26 437.45(4)
$\omega\epsilon$	296.9	241.9	250.2
$\omega\epsilon\chi\epsilon$	1.45(8)	1.85(5)	1.29(3)
B_0	0.130 23(2)	0.121 76(5)	0.120 52(2)
B_1	0.129 95(3)	0.121 33(10)	0.120 54(2)
r_e, Å	2.413	2.496	2.509
α_e	2.7×10^{-4}	4.3×10^{-4}	
$D_e \times 10^{7}$[b]	1.02	1.23	1.12
D^e, eV	1.88	0.98	1.51

[a] All values are given in cm^{-1}, unless otherwise indicated. [b] Calculated using the Kratzer relation.

Molecular constants obtained in this work are listed in Table 6 and paint a quantitatively and qualitatively consistent picture of the bonding in the three states. The ground state, which is bound by 1.88 eV, has a vibrational frequency of 296.9 cm^{-1} with an associated anharmonicity of 1.45 cm^{-1}. The B state, however, is bound by only ca. 1 eV and possesses an appropriately lower vibrational frequency of 241.9 cm^{-1}. The C state, which is bound by 1.5 eV, has a vibrational frequency of 250.2 cm^{-1}, which is appropriately in between the B and X state values. Vibrational constants obtained indicate an 19% and 15% decrease for the B and C state vibrational frequencies upon electronic excitation, respectively, in qualitative agreement with the respective binding energies. Similarly, the rotational constants are in qualitative agreement with the vibrational frequencies, although the B state value of 0.121 76 cm^{-1} is slightly larger than the C state value of 0.120 52 cm^{-1}. This violation of Badger's rule is most likely due to subtle bonding differences between the two states. Results of a standard FC analysis for the C−X and B−X systems are shown in Figure 16a, assuming a vibrational temperature of 300 K. The predicted relative intensities are in excellent agreement with the experimental values shown in Figure 16b and are consistent with the molecular constants derived from our spectral analysis.

Comparison of the AgSi data with the CuSi data presented above indicates interesting similarities between the two coinage metal silicides. For both molecules, our data indicate either $^2\Sigma$ or $^2\Pi$ ground states with similar ground-state bond lengths and nearly identical force constants. Additionally, the 1.88 eV value of the well depth of AgSi is in excellent agreement with the 1.80 eV mass spectrometric value obtained by Riekert et al.[89] and is also consistent with the binding energy for CuSi also obtained in this same work. These bonding trends are qualitatively understood by considering the properties of the constituent atoms that are listed in Table 7.

Comparison of the electronegativity of the individual atoms predicts that the resultant molecular bonds for both AgSi and CuSi will be almost entirely covalent, with virtually no ionic character. Therefore, the diatom bond lengths of the various combinations should be very close to the sums of the individual covalent radii. If we add the covalent radii of Cu and Si, a value of 2.23 Å is obtained, while for

Table 7. Atomic Properties for Ground-State Si, Cu, and Ag

atom	Si	Cu	Ag
atomic radius[a] (Å)	1.46	1.57	1.75
dimer radius/2[b] (Å)	1.12	1.11	1.26
electronegativity	1.90	1.90	1.93

[a] Quantum mechanical value. [b] Experimental values (covalent radius).

AgSi, this sum equals 2.38 Å. These values are very close to the 2.28 and 2.40 Å bond lengths extracted from our data. These studies indicate bonding trends for the first two coinage metal silicides, which are further demonstrated in studies of gold silicides.

Gold Silicide

As is the case with copper and silver silicides, current research on gold silicides has focused primarily on solid-state properties. In particular, the electronic properties of gold−silicon compounds and interfaces has been studied,[91] including the measurement of Schottky diode barrier behavior in copper-doped Au−Si films.[93] Metastable Au−Si structures have been proposed to exist in gold silicide thin films.[93] The presence of Au−Si nanoclusters has been established with high-resolution TEM studies, which indicated the formation of spherical structures under proper annealing conditions.[94] Similar to copper silicides, evidence for electromigration of Au into Si lattices has been obtained,[95] although the mechanism for this effect is not well characterized. Although many solid-state studies of gold silicides exist, only a handful of gas-phase experiments have been performed.

The only gas-phase gold silicide that has been studied to date is the AuSi diatom. The first published data of AuSi consist of a brief report on the vibronically resolved emission spectra for two near-infrared band systems by Barrow et al.[96] in 1964. In this low-resolution work, spectra measured in the 790 nm region were assigned as a $^2\Sigma-X^2\Pi$ system, based on the qualitative appearance of Q-branch heads. However, the congested spectra could not be entirely assigned to a single vibronic progression and were complicated by the presence of both red and blue degraded bandheads. Nonetheless, a ground-state frequency of 391 cm^{-1} was reported. These bands were later reinvestigated by Houdart and Schamps,[97] who also proposed a $^2\Sigma-X^2\Pi$ vibronic assignment. In addition to the near-infrared bands, a band system between 700 and 760 nm was observed and yielded vibrational constants for the ground and excited states of 390.9 and 389.5 cm^{-1}, respectively. The two band systems were assigned as $A^2\Sigma-X^2\Pi_{1/2}$ and $A^2\Sigma-X^2\Pi_{3/2}$. The 750 nm system was reinvestigated later by Coquant and Houdart,[98] who, again, proposed a $^2\Sigma-X^2\Pi$ assignment. In this work, rotational analysis of the 0−0 and 1−1 bands of the $A-X_1$ system yielded rotational constants (and bond lengths) of 0.0617 cm^{-1} (3.34 Å) and 0.0637 cm^{-1} (3.29 Å) for the A and X_1 states, respectively. CRLAS data of AuSi obtained in the UV[53] suggests reassignment of the rotational constants as well as the possibility of reassignment of the ground-state symmetry.

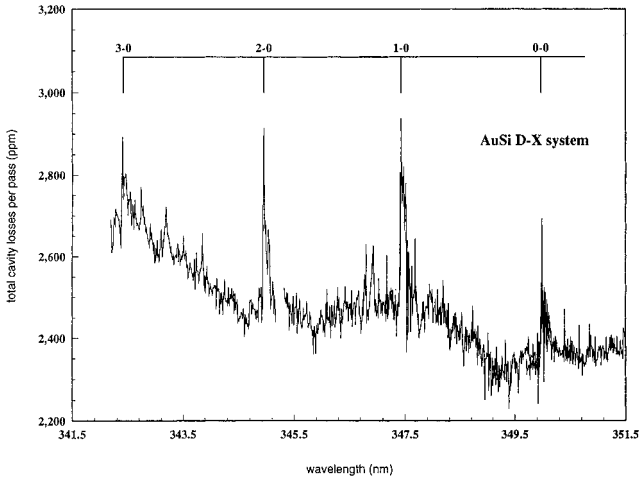

Figure 18. Partial spectrum of the D−X system of AuSi observed at low (0.3 cm^{-1}) resolution. This spectrum is a composite of four separate scans wherein 16 laser shots per wavelength point are averaged. The sloping base line is due to the variation in mirror reflectivity, and the noise is primarily due to scattering losses encountered in the molecular beam, which are significant in this spectral region.

CRLAS spectra were obtained in the same UV region where spectra of copper and silver silicides were obtained. Of the 15 bands measured in the 340−365 nm region, nine have been assigned to vibronic transitions of AuSi, as partially shown in the low resolution scan of Figure 18. Rotationally resolved bands of this system again lacked Q-branches, indicating $\Delta\Lambda(\Omega) = 0$ transitions. The D label for the upper state in this system has been chosen on the basis of several factors. The A state had been assigned to the two band systems previously mentioned. Since no evidence of common upper states was obtained in the previous work, we reserve the B state as possibly belonging to the 750 nm system that was assigned as $A^2\Sigma-X^2\Pi_{1/2}$. Finally, we reserve the C state designation as possibly belonging to three currently unassigned bands observed by us in the 390 nm region.

The most striking result of the vibronic analysis is the large decrease (∼50%) in vibrational frequency upon excitation into the upper electronic state, consistent with the extremely sharp R-branch heads evident in the rotationally resolved data. In addition to the assigned bands, there exist four unassigned bands that are slightly blue shifted with respect to the D state bands. Attempts to fit these bands to a vibrational progression resulted in a negative anharmonic constant. An alternative explanation for these bands will be presented later, following the results of a Franck−Condon analysis.

All of the bands of the D−X system lack Q-branches, indicating $\Delta\Lambda(\Omega) = 0$ transitions. The (2−0) band was rotationally fit as a $^2\Sigma-^2\Sigma$ band, based on the arguments presented above for AgSi and CuSi. The (2−0) rovibronic band was fit for a wide range of rotational assignments by incrementally shifting the rotational quantum numbers. This was done for two reasons: the first was to see if the lower state constants given by Houdart et al. could be reproduced with any assignment. The second reason was to test the measured band intensities using the associated

Table 8. Rotational Constants and Corresponding Bond Lengths Obtained by Incrementally Shifting the Rotational Assignment[a]

line, assignment	$B''\nu$ (cm^{-1}) → $r''\nu$ (Å)		$B'\nu$ (cm^{-1}) → $r'\nu$ (Å)	
28 910.736, **P(2)**	0.1726	1.98	0.1536	2.12
10.736, **P(3)**	0.1536	2.12	0.1347	2.26
10.736, **P(4)**[b]	0.1346	2.26	0.1156	2.44
10.736, **P(5)**	0.1157	2.43	0.0967	2.67
10.736, **P(6)**	0.0976	2.65	0.0787	2.95

[a] Under no circumstance could the rotational assignment of ref 98 be obtained. [b] Indicates final chosen assignment.

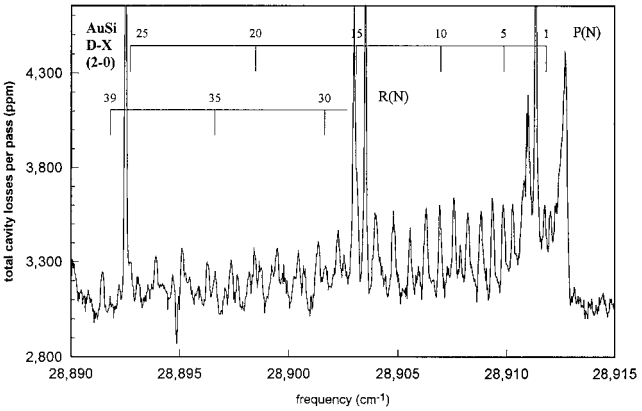

Figure 19. Rotationally resolved 2−0 band of the AuSi D−X system scanned at high (0.04 cm^{-1}) resolution. The rotational assignment is indicated in the figure. The additional large peaks evident in the scan are due to AuH.

Table 9. Molecular Constants for the D−X System of AuSi

	X	*D*
B_ν	0.1350(1) ($\nu = 0$)	0.1161(1) ($\nu = 2$)
$r_{\nu,\text{Å}}$	2.257	2.434
ω_ϵ	401.5(3)	211.44(5)
$\omega_\epsilon\chi_\epsilon$	5.5	1.012
D_e ($\times 10^7$)	0.61[a]	1.4[a]
D^e, eV	3.3[b]	1.37

[a] Values estimated using the Kratzer relation. [b] Value taken from the mass spectrometric dissociation experiments of ref 100.

bond lengths and vibrational frequencies in a Franck−Condon analysis. The results of several of these fits are summarized in Table 8. The conclusion drawn from the constants listed in the table is that if our bands originate from the ground state, then the previous assignment by Coquant and Houdart must be in error, since it is not possible for us to obtain a lower state rotational constant close to their 0.0617 cm^{-1} reported value. This is not surprising, since the 3.3 Å bond length calculated from this rotational constant is much longer than expected based on comparison to the 2.23 and 2.40 Å bond lengths of CuSi and AgSi, respectively, or would be expected from a simple Pauling bonding model[99] The chosen rotational assignment is indicated in Figure 19.

Molecular constants derived from the CRLAS data are presented in Table 9. Using these constants, several Franck−Condon analyses have been performed that included the bond lengths associated with the different rotational assignments of Table 8. In each case, the measured band intensities are different from those predicted. The largest discrepancy is that the intensities of the upper state progression fall off much more rapidly than expected. The FC simulation based on the chosen fit predicts that the 3−0 band will be the most intense, while the experimental data show the 2−0 as the strongest. One possibility for the intensity anomalies associated with the upper state progression is that the upper state is perturbed. Evidence for this suggestion is provided by the additional bands previously mentioned that grow in to the blue of the fundamental progression, located at 28496.7, 28707, 28915.5, and 29128 cm^{-1}. Attempts to fit these bands to a separate regular vibronic progression or as possible hotbands were unsuccessful. One possibility for these additional bands is that strong vibronic mixing with an additional upper electronic state is occurring, which would also explain the discrepancy between the observed band intensities and those predicted in the standard two state F−C analysis. In support of this hypothesis are the relative intensities of bands that terminate on common $\nu = 0$ states of the D state. These band intensities are closer to those predicted in the FC analysis, suggesting that higher vibrational levels of the upper electronic state are more strongly mixed or perturbed. Ab initio calculations as well as data obtained with other techniques in this region would greatly assist in positive assignment of these additional features. In light of the above considerations, only the D−X system is confidently assigned at this time.

From the CRLAS data presented above, regular bonding trends emerge for the three coinage metal silicide diatoms. All of the coinage metal silicide spectra discussed here have a distinct $\Delta\Lambda = 0$ band structure, which suggest either $^2\Sigma$ or $^2\Pi$ ground states, as previously discussed. Resolution of the proper ground-state assignment will likely be resolved in future studies. Extension of the trends presented for AgSi and CuSi (see Table 7) to include Au explains the stronger bonding character of AuSi. The difference in electronegativity between Au and Si is ca. 0.6, which leads to an expected ionic bonding contribution of ca. 10%. This increased bond strength is evidenced by the increased force constant of AuSi derived from the ground-state vibrational frequency. Similarly, the 2.26 Å bond length of AuSi is slightly less than the sum of the two atomic covalent radii, as expected, and is appropriately less than that of AgSi. These points are also in agreement with the measured dissociation energy of 3.3 eV obtained by Gingerich,[100] which is substantially larger than the dissociation energies of both CuSi and AgSi.

From the CRLAS data, we have extracted bond lengths, force constants, and binding energies of the diatomic silicide species that will serve as a benchmark for larger cluster studies and for ab initio predictions. The ground-state properties derived from the data and discussions presented here are important in understanding the detailed bonding of metal silicide species. Studies of silicides that contain transition metals from other columns of the periodic table would provide an interesting test of the conclusions drawn from this work. Recent results[54] on the PtSi diatom obtained in our lab are again consistent with the above observed trends, with an

additional bonding contribution from the d-hole observed.

V. Summary

In this paper we have presented an overview of the history, theory, and practice of the CRLAS technique, with emphasis on the fundamentals principles underlying the technique and practical examples from our own molecular beam studies. Although currently used by a relatively small number of researchers in the near UV to mid-IR regions, the increased availability of highly reflective optics will expand its usage as well as facilitate the extension to new wavelength regimes. With the development of more sophisticated detection schemes, technique sensitivity can be further improved, provided careful consideration is given to the potential effects of transverse and longitudinal mode competition in the resonator.

Results for several species generated by laser vaporization and cooled in supersonic jets have been presented and indicate the generality of the ringdown method for the study of transient species. The advantages associated with CRLAS in comparison to established techniques have been underscored and result principally from the fact that CRLAS is a direct absorption technique and is therefore relatively free from the complications and limitations associated with molecular internal conversion and excited state predissociation. The ability to measure states that are not accessible with established "action" techniques has been demonstrated with the aluminum dimer spectra, while the intensity distortions which can be introduced due to intramolecular dynamics have been presented in the Cu_2 and Cu_3 data. Finally, the results of the application of CRLAS to the study of metal silicides indicates the power of the method for the spectroscopic characterization of new species. All of the above studies exhibit high sensitivity levels similar to those of the other methods that have been historically implemented for that reason. Extension of the work presented here to include larger clusters and ions is limited only by the ability to produce high enough concentrations in the ringdown probe laser region. This presents many exciting possibilities for future work, since resonance ionization techniques are not suited for obtaining optical spectra for metal cluster ions, and in both neutrals and ions, the possibility of excited-state nonradiative relaxation typically increases with increasing cluster size.

As CRLAS is a relatively new technique, it is likely to become more widely used in the years to come, as improvements in wavelength coverage and sensitivity are made. The most compelling attributes of the method are its simplicity and versatility, combined with an extraordinarily high sensitivity. The applications and developments outlined in this review imply an exciting future for the CRLAS technique in an increasing number of applications. We hope that this paper facilitates such further developments.

VI. Acknowledgments

This research was supported by The HEDM program of the AFOSR (Grant No. F49620-93-1-0278). Equipment was supplied by the Research Fund of the American Chemical Society (Grant No. 24049-AC6) and the National Science Foundation (Grant No. CHE-9424482). J.J.S. thanks IBM for a predoctoral fellowship. We would also like to acknowledge the many helpful suggestions of the reviewers as well as insightful discussions with Dr. Carl Weimann.

VII. References

(1) Herbelin, J. M.; McKay, J. A.; Kwok, M. A.; Ueunten, R. H.; Urevig, D. S.; Spencer, D. J.; Benard, D. J. *Appl. Opt.* **1980**, *19*(1), 144.
(2) Herbelin, J. M.; McKay, J. A. *Appl. Opt.* **1980**, *20*(19), 3341.
(3) Kwok, M. A.; Herbelin, J. M.; Ueunten, R. H. *Opt.* **1982**, *Eng. 21*, 979.
(4) Anderson, D. Z.; Frisch, J. C.; Masser, C. S. *Appl. Opt.* **1984**, *23*(8), 1238.
(5) O'Keefe, A.; Deacon, D. A. G. *Rev. Sci. Instrum.* **1988**, *59* (12), 2544. See also: Ramponi, A. J.; Milanovich, F. P.; Kan, T.; Deacon, D. *Appl. Opt. 27*(22), 4606.
(6) O'Keefe, A.; Scherer, J. J.; Cooksy, A. L.; Sheeks, R.; Heath, J.; Saykally, R. J. *Chem. Phys. Lett.* **1990**, *172* (3), 214.
(7) Heath, J. R.; Cooksy, A. L.; Gruebele, M. H. W.; Schmuttenmaer, C. A.; Saykally, R. J. *Science* **1989**, *244*, 564.
(8) Benard, D. J.; Winker, K. B. *J. Appl. Phys.* **1991**, *69*, 2805.
(9) Yu, T.; Lin, M. C. *J. Am. Chem. Soc.* **1993**, *115*, 4371.
(10) Yu, T.; Lin, M. C. *J. Phys. Chem.* **1994**, *98*, 2105.
(11) Yu, T.; Lin, M. C. *J. Phys. Chem.* **1994**, *98*, 9697.
(12) Diau, E. W.; Yu, T.; Wagner, M. A. G.; Lin, M. C. *J. Phys. Chem.* **1994**, *98*, 4034.
(13) Zhu, L.; Johnston, G. *J. Chem Phys.* **1995**, *99*, 15114.
(14) Romanini, D.; Lehmann, K. K. *J. Chem. Phys.* **1993**, *99*, 6287.
(15) Romanini, D.; Lehmann, K. K. *J. Chem. Phys.* **1995**, *102*, 633.
(16) Meijer, G.; Boogaarts, M. G. H.; Jongma, R. T.; Parker, D. H.; Wodtke, A. M. *Chem. Phys. Lett.* **1994**, *217*, 112.
(17) Jongma, R. T.; Boogaarts, M. G. H.; Holleman, I.; Meijer, G. *Rev. Sci. Instrum.* **1995**, *66*, 2821.
(18) Jongma, R. T.; Boogaarts, M. G. H.; Meijer, G. *J. Mol. Spectrosc.* **1994**, *165*, 303.
(19) Boogaarts, M. G. H.; Meijer, G. *J. Chem. Phys.* **1995**, *103*, 5269.
(20) Zalicki, P.; Ma, Y.; Zare, R. N.; Wahl, E. H.; Owano, T. G.; Harris, J. S.; Kruger, C. H. *Chem. Phys. Lett.* **1995**, *234*, 269.
(21) Sick, V.; Farrow, R. L. *Opt. Lett.* **1995**, *11*, 111.
(22) Scherer, J. J.; Voelkel, D.; Rakestraw, D. J.; Paul, J. B.; Collier, C. P.; Saykally, R. J.; O'Keefe, A. *Chem. Phys. Lett.* **1995**, *245*, 273.
(23) Scherer, J. J.; Voelkel, D.; Rakestraw, D. J. *Appl. Phys. B*, submitted.
(24) Scherer, J. J.; Voelkel, D.; Rakestraw, D. J. Paper presented at the *51st Ohio State University Symposium on Molecular Spectroscopy*, 1996.
(25) Scherer, J. J.; Rakestraw, D. J. *Chem. Phys. Lett.*, submitted.
(26) Paul, J. B.; Collier, C. P.; Scherer, J. J.; O'Keefe, A.; Saykally, R. J. *Science*, submitted.
(27) Engeln, R.; Meijer, G. Paper presented at the *51st Ohio State University Symposium on Molecular Spectroscopy*, 1996.
(28) Giles, B.; Arrington, C. A.; Hagemeister, F. C.; Zwier, T. S. Paper presented at the *51st Ohio State University Symposium on Molecular Spectroscopy*, 1996.
(29) Pearson, J.; Orr-Ewing, A. J.; Ashfold, M. N. R.; Dixon, R. N. *J. Chem. Soc., Faraday Trans.* **1996**, *92*, Apr 7, N7: 1283−1285.
(30) Zalicki, P.; Zare, R. N. *J. Chem. Phys.* **1995**, *102*, 2708.
(31) Hodges, J. T.; Looney, P.; van Zee, R. D. *Appl. Opt. 1995*, *35*, 4112.
(32) Siegman, A. *Lasers*; University Science Books: Mill Valley, CA, 1986.
(33) Scherer, J. J.; Paul, J. B.; O'Keefe, A.; Saykally, R. J. In *Advances in Metal and Semiconductor Clusters*: Duncan, M.; Ed.; JAI Press: Greenwich, 1995; Vol. VIII, pp 149−180.
(34) Martin, J.; Paldus, B. A.; Zaliki, P.; Wahl, E. H.; Owano, T. G.; Harris, J. S.; Kruger, C. H.; Zare, R. N. *Chem. Phys. Lett.* **1996**, *258*, 63.
(35) Lehmann, K. K.; Romanini, D. Paper presented at the *51st Ohio State University Symposium on Molecular Spectroscopy*, 1996.
(36) Kogelnik, H.; Li, T. *Appl. Optics* **1966**, *5*, 1550.
(37) See, e.g.: Heurtley, J. C.; Striefer, W. *J. Op. Soc. Am.* **1965**, *55*, 1472.
(38) See, e.g.: Li, T. *Bell Sys. Tech. J.* May, 1965.
(39) See, e.g.: Hecht, E.; Zajac, A. *Optics*; Addison Wesley: Reading, MA, 1987; p 2835.
(40) The previous treatment is modeled after ref 32, Chapter 27.
(41) Ramsey, N. F. *Molecular Beams, 2nd ed.*; Clarendon: Oxford, 1989.
(42) Teets, R.; Eckstein, J.; Hänsch, T. W. *Phys Rev. Lett.* **1977**, *38*, 760.

(43) Salour, M. M. In *Laser Spectroscopy III*; Hall, J. L., Carlsten, J. L., Eds.; Springer-Verlag: New York, 1977.
(44) Bergquist, J. C.; Lee, S. A.; Hall, J. L. Ref 43, p 142.
(45) Crisp, M. D. *Phys. Rev. A.* **1970**, *1*, 1604.
(46) Hodges, J. T.; Looney, P.; van Zee, R. *J. Chem. Phys.*, submitted.
(47) See, e.g.: Fox, A. G.; Li, T. *Bell Syst. Tech. J.* March 1961, 453.
(48) See, e.g. Demtröder, W. *Laser Spectroscopy*; Springer Verlag: New York, 1981; p 163.
(49) Paul, J. B.; Scherer, J. J.; Collier, C. P.; Saykally, R. J. Manuscript in preparation.
(50) Scherer, J. J.; Paul, J. B.; Saykally, R. J. *Chem. Phys. Lett.* **1995**, *242*, 395.
(51) Scherer, J. J.; Paul, J. B.; Collier, C. P.; Saykally, R. J. *J. Chem. Phys.* **1995**, *102*, 5190.
(52) Scherer, J. J.; Paul, J. B.; Collier, C. P.; Saykally, R. J. *J. Chem. Phys.* **1995**, *103*, 113.
(53) Scherer, J. J.; Paul, J. B.; Collier, C. P.; Saykally, R. J. *J. Chem. Phys.* **1995**, *103*, 9187.
(54) Paul, J. B.; Scherer, J. J.; Collier, C. P.; Saykally, R. J. *J. Chem. Phys.* **1996**, *104*.
(55) See, e.g.: Weltner, W., Jr.; van Zee, R. J. *Ann. Rev. Phys. Chem.* **1984**, *35*, 291.
(56) See, e.g.: Selby, K.; Vollmer, M.; Masui, J.; Kresin, V.; de Heer, W. A.; Knight, W. D. *Phys. Rev. B* **1989**, *40*, 5417.
(57) See, e.g.: Kappes, M. M. *Chem. Rev.* **1988**, *88*, 369.
(58) See, e.g.: Bondebey, B. E.; English, J. H. *J. Chem. Phys.* **1981**, *74*, 6978.
(59) Gole, J. L.; English, J. H.; Bondybey, V. E. *J. Phys. Chem.* **1982**, *86*, 2560.
(60) Powers, D. E.; Hansen, S. G.; Geusic, M. E.; Pulu, A. C.; Hopkins, J. B.; Dietz, T. G.; Duncan, M. A.; Langridge-Smith, P. R. R.; Smalley, R. E. *J. Phys. Chem.* **1982**, *86*, 2556.
(61) Page, R. H.; Gudemann, C. S. *J. Chem. Phys.* **1991**, *94*, 39.
(62) Fu, Z.; Lemire, G. W.; Bishea, G. A.; Morse, M. D. *J. Chem. Phys.* **1990**, *93*, 8420.
(63) Cai, M. F.; Carter, C. C.; Miller, T. A.; Bondybey, V. E. *Chem. Phys.* **1991**, *155*, 233.
(64) Langhoff, S. R.; Bauschlicher, C. W. *J. Chem. Phys.* **1990**, *92*, 1879.
(65) Douglas, M. A.; Hauge, R. H.; Margrave, J. L. *J. Phys. Chem.* **1983**, *87*, 2945.
(66) Moskovits, M.; Hulse, J. E. *J. Chem. Phys.* 1977, *67*, 4271.
(67) Morse, M. D.; Hopkins, J. B.; Langridge-Smith, P. R. R.; Smalley, R. E. *J. Chem. Phys.* **1983**, *79*, 5316.
(68) Rohlfing, E. A.; Valentini, J. J. *Chem. Phys. Lett.* **1986**, *126*, 113.
(69) Bauschlicher, C. W.; Langhoff, S. R.; Taylor, P. R. *J. Chem. Phys.* **1987**, *88*, 1041.
(70) Knicklebein, M. B. *J. Chem. Phys.* **1994**, *100*, 4729.
(71) See, e.g.: Ng, K. K. *Properties of Silicon*; EMIS data reviews series #4; INSPEC: London, U.K., 1988; pp 799−826.
(72) Cabrera, A. L.; Kirner, J. F.; Armor, J. N. *J. Mater. Res.* **1990**, *6*, 71.
(73) Hymes, S.; Muraka, S. P.; Shepard, C.; Langford, W. A. *J. Appl. Phys.* **1992**, *71*, 4623.
(74) Setton, M.; Van der Spiegel, J.; Rothman, B. *Appl. Phys. Lett.* **1990**, *57*, 357.
(75) Padiyath, R.; Seth, J.; Babu, S. V.; Matienzo, L. J. *J. Appl. Phys.* **1993**, *73*, 2326.
(76) Aboelfotoh, M. O.; Cros, A.; Stevenson, B. G.; Tu, K. N. *Phys. Rev. B* **1990**, *41*, 9819.
(77) Shim, I.; Kingcade, J. E., Jr.; Gingerich, K. A. *Z. Phys. D−Atoms, Mol. Clusters* **1987**, *7*, 261.
(78) Shim, I.; Gingerich, K. A. *Z. Phys. D−Atoms, Mol. Clusters* **1990**, *16*, 141; *Int. J. Quant. Chem.* **1989**, *S23*, 409.
(79) Haberlandt, H.; *Chem. Phys. 138*, 315.
(80) Bishea, G. A.; Arrington, C. A.; Behm, J. M.; Morse, M. D. *J. Chem. Phys.* **1991**, *95*, 8765.
(81) Herzberg, G.; *Spectra of Diatomic Molecules*; D. Van Nostrand: New York, 1953; Chapter VI.
(82) Xide, X.; Kaiming, Z. *Prog. Surf. Sci.* **1988**, *28*, 71.
(83) Kambli, U.; von Allmen, M.; Saunders, N.; Miodownik, A. P. *Appl. Phys. A* **1985**, *A36*, 189.
(84) Hassam, S.; Gaune-Escard, M.; Bros, J. P. *Ber. Bunsen. Fur Physik. Chem.* **1983**, *87*, 785.
(85) Le Lay, G. *J. Vac. Sci. Technol. B* **1983**, *1*, 354.
(86) Arnold, M.; Fruhauf, J.; Schneider, H. G. *Cryst. Res. Technol.* **1983**, *18*, 1015.
(87) Tokutaka, H.; Nishimori, K.; Nomura, S.; Tanaka, A.; Takashima, K. *Surf. Sci.* **1982**, *115*, 79.
(88) Budinavicius, J.; Pranevicius, L.; Tamulevicius, S. *Phys. Status Solidi A* **1989**, *114*, K25.
(89) Riekert, G.; Lamparter, P.; Steeb, S. *Z. Metall.* **1981**, *72*, 765.
(90) Gausset, L.; Herzberg, G.; Lagerqvist, A.; Rosen, B. *Astrophys. J.* **1965**, *142*, 45.
(91) Bisi, O.; Calandra, C.; Braicovich, L.; Abbati, I. *J. Phys. C* **1982**, *15*, 4707.
(92) Toyama, N. *J. Appl. Phys.* **1984**, *55*, 4398.
(93) Dhere, N. G.; De A. Loural, C. *Thin Solid Films* **1981**, *81*, 213.
(94) Baumann, F. H.; Schroter, W. *Phys. Rev. B* **1991**, *43*, 6510.
(95) Christou, A. Conference paper, 5th Spring Meeting of AIME, **1983**; p 149.
(96) Barrow, R. F.; Gissane, W. J. M.; Travis, D. N. *Nature* **1964**, *201*, 603.
(97) Houdart, R.; Schamps, J. *J. Phys B* **1973**, *6*, 2478.
(98) Coquant, C.; Houdart, R. *C. R. Acad. Sci. Paris* **1977**, *284*, 171.
(99) Pauling, L. *J. Am. Chem. Soc.* **1947**; *69*, 542.
(100) Gingerich, K. A. *J. Chem. Phys.* **1969**, *50*, 5426.

CR930048D